International Journal of
Molecular Sciences

MDPI

Article

FOXC1 Regulates Cytokine Signaling, Inflammatory Pathways, and Retinoid Metabolism to Maintain Limbal Epithelial Cell Homeostasis In Vitro

Swarnali Kundu [1], Maryam Amini [1], Tanja Stachon [1,2], Fabian Norbert Fries [1,3], Berthold Seitz [3], Zhen Li [1], Shuailin Li [1,2], Shanhe Liu [1,2], Shao-Lun Hsu [1,2], Shweta Suiwal [1,2] and Nóra Szentmáry [1,2,4,*]

[1] Dr. Rolf M. Schwiete Center for Limbal Stem Cell and Congenital Aniridia Research, Saarland University, 66424 Homburg/Saar, Germany; s8swkund@uni-saarland.de (S.K.); maryam@amini.cloud (M.A.); tanja.stachon@uni-saarland.de (T.S.); fabian.fries@uks.eu (F.N.F.); zhen.li@uks.eu (Z.L.); shuailinli97@gmail.com (S.L.); liushanhe666@gmail.com (S.L.); arinahsu@gmail.com (S.-L.H.); shweta.suiwal@uni-saarland.de (S.S.)
[2] Department of Experimental Ophthalmology, Saarland University, 66424 Homburg/Saar, Germany
[3] Department of Ophthalmology, Saarland University Medical Center, 66424 Homburg/Saar, Germany; berthold.seitz@uks.eu
[4] Department of Ophthalomology, Semmelweis University, 1085 Budapest, Hungary
* Correspondence: nora.szentmary@uni-saarland.de

Abstract

This study aimed to evaluate FOXC1-mediated regulatory mechanisms on gene and protein expression profiles in primary human limbal epithelial cells (pLECs) using siRNA-mediated FOXC1 knockdown under basal conditions and following lipopolysaccharide (LPS) and interleukin-1β (IL-1β)-induced inflammatory conditions. The gene expression related to inflammation, epithelial differentiation, cell proliferation and remodeling, and retinoic acid metabolism was analyzed using qPCR. Corresponding protein levels were assessed through Western blotting and ELISA. FOXC1 silencing significantly downregulated epithelial differentiation markers KRT12 and KRT13 at the mRNA and protein levels ($p \leq 0.045$), whereas KRT3 and KRT19 were unaffected. Inflammatory signaling was markedly altered, with a reduced *IL-6* and *IL-8* mRNA expression ($p \leq 0.029$), increased IL-1α expression ($p \leq 0.015$), and condition-dependent changes in IL-6 and IL-8 protein secretion. *CCL2* was increased at the mRNA level only ($p = 0.007$). *VEGFA* mRNA was consistently reduced ($p \leq 0.022$) without corresponding protein changes, while TGF-β protein was increased under non-inflammatory and LPS conditions ($p \leq 0.011$). Genes involved in retinoid metabolism, including *CYP1B1*, *FABP5*, *CRABP2*, *RDH10*, *STRA6*, and *ALDH3A1*, were significantly downregulated ($p \leq 0.037$), with reduced CRABP2 and RDH10 protein levels ($p \leq 0.017$) and a decreased FABP5/CRABP2 ratio under IL-1β stimulation ($p = 0.006$). FOXC1 knockdown affected proliferation-related genes, with decreased *FOSL2* ($p = 0.048$) and increased *MKi67* ($p = 0.006$). FOXC1 silencing disrupts epithelial differentiation, inflammatory signaling, retinoid metabolism, and selected proliferation-related pathways at the transcriptional level, with more selective effects on protein levels. Such changes may potentially predispose the ocular surface to lineage instability, fibrosis, and impaired regenerative capacity.

Keywords: FOXC1; human primary limbal epithelial cells; retinoic acid signaling; TGF-β; knockdown

Academic Editor: Jodhbir S. Mehta

Received: 6 January 2026
Revised: 3 February 2026
Accepted: 11 February 2026
Published: 15 February 2026

1. Introduction

The corneal epithelium functions as a protective barrier and represents the first line of defense against environmental insults and pathogens. Corneal integrity, avascularity, and transparency are essential for maintaining visual acuity. Corneal homeostasis is supported by non-keratinized, non-vascularized corneal epithelial cells, which require continuous renewal mediated by limbal epithelial cells (LECs). These LECs are replenished by quiescent, limbal stem cells (LSCs) residing in the limbal stem cell niche, located at the junction between the cornea and the conjunctiva [1,2]. Upon activation, LSCs differentiate into transient amplifying cells that migrate centripetally toward the corneal center, where they proliferate and stratify to regenerate the corneal epithelium, thereby preserving homeostasis, transparency, and avascularity [3–5].

In limbal epithelial cells, cell fate, renewal, and homeostasis are regulated by a complex network of signaling pathways and transcription factors, including the p38 mitogen activated protein kinase (p38 MAPK) signaling pathway [6] and the Hippo/YAP (Yes-associated protein) pathway [7]. Among these, paired box protein 6 (PAX6) is one of the best characterized, acting as a master regulator of ocular cell specification and development. Previous studies have shown that Forkhead box C1 (FOXC1) is co-expressed with PAX6 in the human limbus and corneal epithelium, underscoring its complementary role in maintaining epithelial cell identity [8]. Both FOXC1 and PAX6 reciprocally influence neural crest and ocular development, directing corneal epithelial lineage commitment [8] and embryonic anterior segment formation [9]. The loss of either PAX6 or FOXC1 in the limbal stem cell niche disrupts LSC identity, leading to a keratocyte-like phenotype characterized by the upregulation of epidermal stratification markers. Recent evidence further suggests that FOXC1 functions as a "shared" transcription factor between LSCs and stromal or keratinocyte lineages, with higher expression levels in LSCs, where it regulates stem cell fate and modulates PAX6 activity [2].

The Forkhead box family comprises evolutionarily conserved transcription factors characterized by a ~110-amino-acid Forkhead (winged-helix) DNA-binding domain, which recognizes the consensus sequence GTAAATAAA. Structural studies have revealed distinct N-terminal transactivation, transcriptional inhibitory, and C-terminal activation domains within FOX proteins [10]. FOXC1, a member of this family, regulates embryogenesis, cell migration, differentiation, and cell fate determination by binding specific DNA motifs and interacting with other transcriptional regulators. In the cornea, FOXC1 controls corneal epithelial cell fate, modulates the keratinization switch, and maintains the limbal stem cell niche [8,11–13]. FOXC1 missense mutations, deletions, and duplications are linked to Axenfeld–Rieger syndrome, which presents with corneal neovascularization, anterior segment dysgenesis, and systemic abnormalities such as dental and hearing defects [14–17]. Beyond the eye, FOXC1 is expressed in the heart, kidney, leukocytes, and prostate, where it acts as a key regulator of embryonic development, including for the brain, bone, and heart [11,18,19]. FOXC1 knockout mice die shortly after birth, exhibiting severe developmental defects and hydrocephalus [19]. In addition, FOXC1 dysregulation has been extensively studied in the context of tumorigenesis and metastasis [14]. Initially identified as a key biomarker overexpressed in triple-negative breast cancer and basal-like breast cancer [20], FOXC1 has since been also recognized as an important regulator of transcriptional activation and repression, translation, and post-translational modification.

Congenital aniridia is a pan-ocular disorder characterized by partial or complete iris hypoplasia, cataract, foveal and optic nerve underdevelopment, and nystagmus. Between others, pathogenic variants in PAX6, FOXC1, paired-like homeodomain transcription factor 2 (PITX2), Cytochrome P450 1B1 (CYP1B1), Forkhead box D3 (FOXD3) and Tripartite motif containing 44 (TRIM44) have been identified in affected patients [21]. Classical

aniridia is caused by heterozygous mutations in PAX6 on chromosome 11p13, whereas aniridia-associated keratopathy (AAK) can also involve FOXC1, PITX2, and CYP1B1 pathogenic variants. Nuclear transcription factors such as PAX6 and FOXC1 regulate LSC identity and fate by binding to regulatory enhancer elements, and their dysfunction contributes to limbal stem cell deficiency (LSCD). FOXC1-related aniridia, mapped to chromosome 6p25 [22], functions downstream of PAX6 and TGF-β signaling [12].

Beyond genetic variants, the ocular surface of aniridia patients exhibits a pro-inflammatory microenvironment. The proteomic analysis of tear fluid has revealed elevated levels of cytokines (CCL3, IL-1β, IL-9, IL-17A) and inflammatory mediators such as eotaxin, bFGF/FGF2, and VEGFA. A disrupted ratio between anti-inflammatory IL-1RA and pro-inflammatory IL-1β further indicated a shift toward chronic inflammation in aniridia [23,24].

In this study, we investigated the previously uncharacterized effects of FOXC1 knockdown on gene and protein levels in human primary LECs (pLECs). To replicate inflammatory conditions in vitro, inflammation was induced using lipopolysaccharide (LPS) and interleukin-1β (IL-1β) to assess the effects of inflammation on FOXC1 siRNA knockdown in pLECs.

2. Results

2.1. FOXC1 mRNA and Proteins Levels in pLECs

The *FOXC1* mRNA level was significantly reduced following FOXC1 siRNA knockdown compared with siRNA controls, both without inflammation ($p < 0.001$) and after the induction of inflammation with LPS or IL-1β ($p < 0.001$). In contrast, FOXC1 protein levels did not differ significantly between FOXC1 siRNA-treated and control siRNA-treated cells, regardless of inflammatory stimulation (LPS or IL-1β) across all treatment groups ($p \geq 0.423$) (Figure 1A–C).

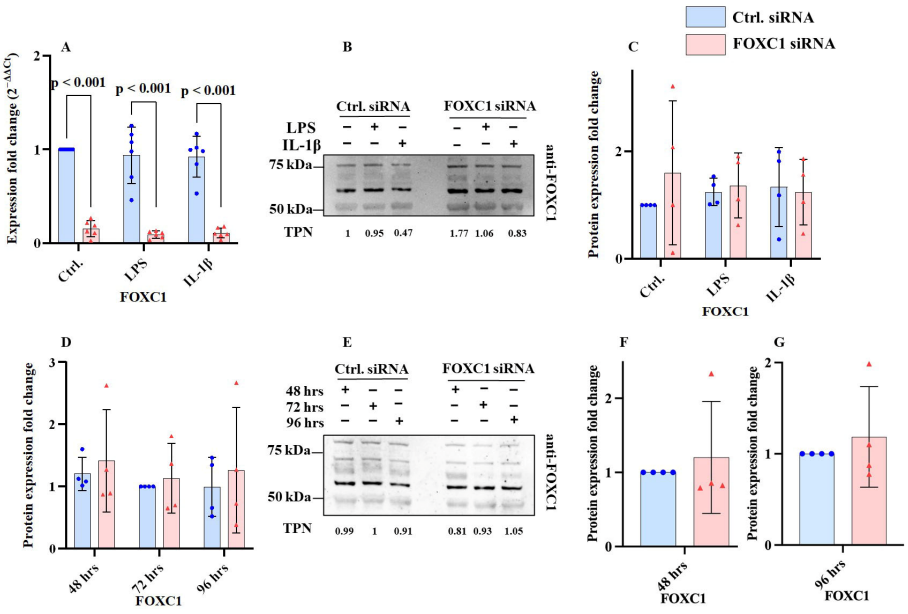

Figure 1. Forkhead box C1 (FOXC1) mRNA and proteins levels ($n = 6$; $n = 5$) in primary human limbal epithelial cells (pLECs) 72 h after transfection with control siRNA (blue) or with FOXC1 knockdown siRNA (pink), without or with lipopolysaccharide (LPS) or interleukin 1β (IL-1β) treatment (**A**–**C**). FOXC1 protein levels in pLECs 48, 72, and 96 h after transfection with control siRNA (blue) or with FOXC1 knockdown siRNA (pink), without LPS or IL-1β treatment ($n = 4$) (**D**–**G**). Data are shown as mean ± SD. Data have been tested for normal distribution with Shapiro–Wilk test. Statistical analysis

has been performed using two-way ANOVA followed by Tukey's post hoc test (**A**–**E**), or statistical analysis has been performed using *t*-test (**F**,**G**). *p*-values below 0.05 were considered statistically significant. Representative Western blot images are also displayed (**B**,**E**). Each data point represents an individual donor. *FOXC1* mRNA levels were significantly lower following FOXC1 siRNA knockdown compared to siRNA controls without ($p < 0.001$) and with induced inflammation (either LPS or IL-1β treatment; $p < 0.001$). However, FOXC1 protein levels were not changed significantly after FOXC1 siRNA knockdown compared to siRNA controls ($p \geq 0.423$) without or with LPS- or IL-1β-induced inflammation with any of the groups (**A**–**C**). FOXC1 protein levels (FOXC1 antibody from Proteintech, Rosemont, IL, USA) were tested at intervals of 48, 72 and 96 h after FOXC1 siRNA knockdown without significant change to the outcome compared to siRNA controls measured at the same time points ($p \geq 0.639$; $p \geq 0.764$; $p \geq 0.552$ for 48, 72, and 96 h, respectively) (**D**,**E**). Comparing FOXC1 siRNA knockdown to siRNA controls at 48 h and 96 h after transfection, with paired two-tailed *t*-test, showed no significant changes ($p \geq 0.199$) (**F**,**G**). Western blots probed with anti-FOXC1 antibodies from additional sources (R&D Biotechne) have been included in Supplementary Figure S1.

The FOXC1 protein level was analyzed at 48, 72, and 96 h post-transfection. No significant differences were detected compared with siRNA controls at any time point ($p \geq 0.189$, respectively) (Figure 1D,E and Supplementary Figure S1A,B). Similarly, a direct comparison between FOXC1 siRNA knockdown and siRNA control samples at 48 and 96 h post-transfection using a paired two-tailed *t*-test revealed no significant changes ($p \geq 0.199$) (Figure 1F,G).

2.2. Cytokeratin mRNA and Protein Levels in pLECs

Cytokeratin mRNA and protein levels are shown at Figure 2A–H. The *KRT12* (cytokeratin 12) mRNA level was significantly reduced following FOXC1 siRNA knockdown compared with siRNA controls, both without and with LPS-induced inflammatory conditions ($p < 0.001$). In addition, *KRT12* mRNA levels were lower in IL-1β-treated siRNA control cells compared with controls without inflammatory stimuli ($p = 0.027$) (Figure 2A). Consistently, the KRT12 protein level was downregulated in FOXC1 knockdown pLECs compared to siRNA controls under IL-1β-induced inflammation ($p = 0.035$) (Figure 2B,C).

Similarly, the *KRT13* (cytokeratin 13) mRNA level was significantly reduced in FOXC1 knockdown LECs relative to siRNA controls in all groups, with or without LPS or IL-1β stimulation ($p < 0.001$). In control siRNA-transfected cells, IL-1β also led to a significant reduction in *KRT13* mRNA levels compared to cells without inflammatory stimuli ($p = 0.002$) (Figure 2D). At the protein level, KRT13 was significantly downregulated in FOXC1 knockdown pLECs without inflammatory stimuli ($p < 0.001$). In addition, LPS- or IL-1β-induced inflammation significantly reduced the KRT13 protein level in control siRNA knockdown pLECs ($p < 0.001$) (Figure 2E,F).

In contrast, KRT3 (cytokeratin 3) and *KRT19* (cytokeratin 19) mRNA levels remained unchanged across all treatment groups, irrespective of inflammatory stimulation ($p \geq 0.179$) (Figure 2G,H).

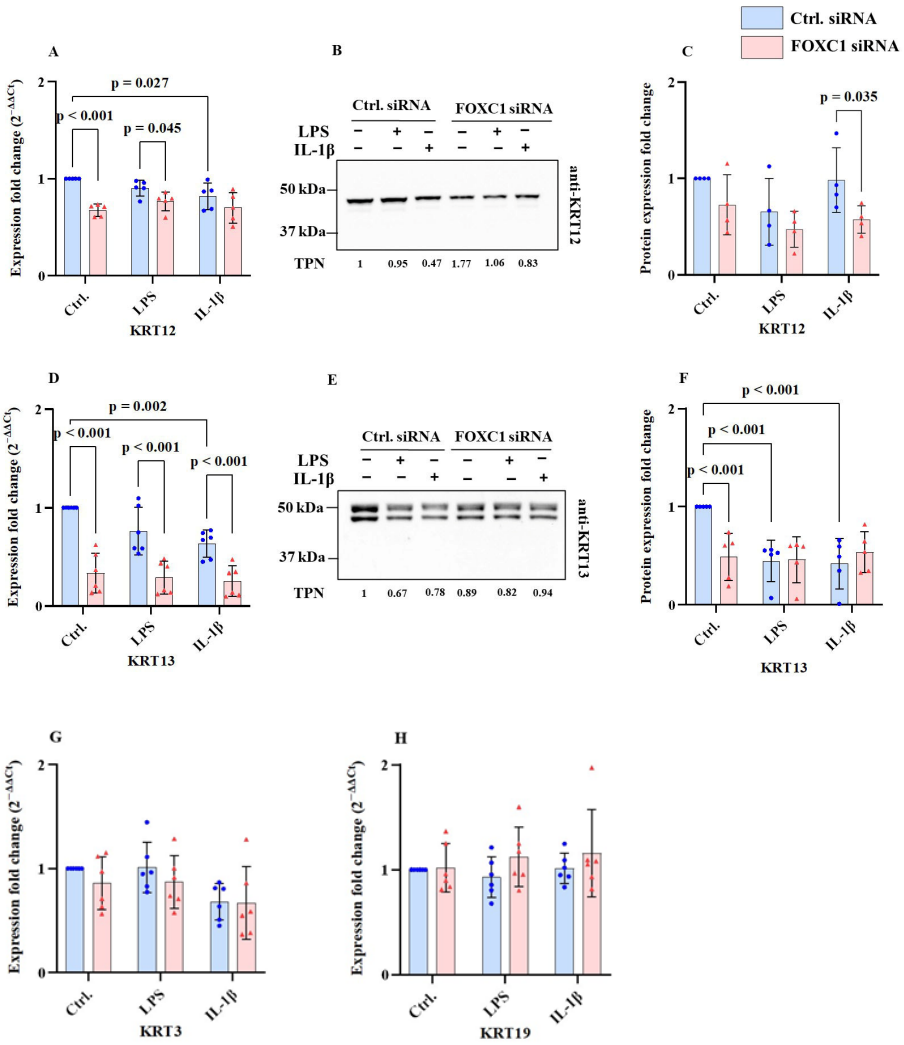

Figure 2. Cytokeratin 12 (KRT12) and cytokeratin 13 (KRT13) mRNA and proteins levels ($n = 6$; $n = 5$); and *cytokeratin 3* (*KRT3*) and *cytokeratin 19* (*KRT19*) mRNA levels in primary human limbal epithelial cells (pLECs) 72 h after transfection with control siRNA (blue) or with FOXC1 knockdown siRNA (pink), without or with lipopolysaccharide (LPS) or interleukin 1β (IL-1β) treatment (**A**–**H**). Data are shown as mean ± SD. Data have been tested for normal distribution using Shapiro–Wilk test. Statistical analysis has been performed using two-way ANOVA followed by Tukey test. *p*-values below 0.05 were considered statistically significant. Representative Western blot images also shown here (**B**,**E**). Each data point represents an individual donor. *KRT12* mRNA levels were significantly downregulated following FOXC1 siRNA knockdown compared to siRNA controls, with and without LPS-induced inflammation ($p \geq 0.001$). Additionally, *KRT12* mRNA levels were significantly lower in IL-1β-induced inflammation in control siRNA-transfected cells compared to non-inflamed conditions ($p = 0.027$). (**A**) In FOXC1 knockdown pLECs, KRT12 protein levels are downregulated compared to siRNA controls with IL-1β-induced inflammation ($p = 0.035$) (**B**,**C**). *KRT13* mRNA levels were downregulated in FOXC1 knockdown pLECs compared to siRNA controls without and with LPS or IL-1β ($p < 0.001$). *KRT13* mRNA levels were significantly lower in IL-1β-induced inflammation in control siRNA-transfected cells compared to non-inflamed conditions ($p = 0.002$) (**D**). KRT13 protein levels were significantly downregulated in FOXC1 knockdown pLECs compared to siRNA controls without inflammation ($p < 0.001$). Additionally, KRT13 protein levels were significantly lower in LPS- or IL-1β-induced inflammation in control siRNA-transfected cells compared to non-inflamed conditions ($p < 0.001$) (**E**,**F**). Supplementary Figure S2 shows the corresponding TPN quantification image for the anti-KRT13-probed blot in (**E**). *KRT3* and *KRT19* mRNA levels did not show significant changes between any of the groups, without or with inflammatory treatment ($p \geq 0.179$) (**G**,**H**).

2.3. Interleukin mRNA and Protein Levels in pLECs

Interleukin mRNA and protein levels are displayed in Figure 3A–F. FOXC1 siRNA knockdown significantly reduced pre/pro-inflammatory cytokine interleukin-6 (IL-6) mRNA and protein both without and with inflammatory conditions (LPS or IL-1β) compared with siRNA controls ($p \leq 0.011$). However, in FOXC1 knockdown pLECs treated with IL-1β, the IL-6 protein level was significantly higher than in cells exposed to LPS ($p = 0.022$) or cells without conditions ($p = 0.002$). Similarly, IL-6 protein levels were elevated in control siRNA pLECs after IL-1β stimulation compared with cells without inflammatory stimuli ($p = 0.009$) (Figure 3A,D).

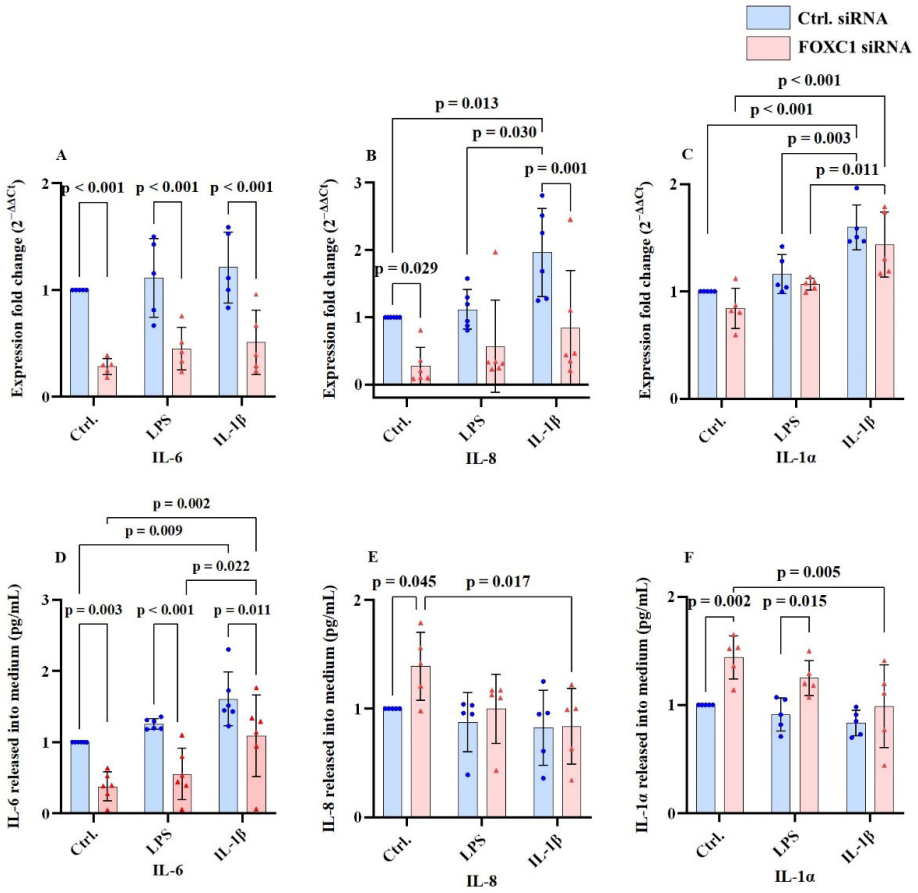

Figure 3. Interleukin 6 (IL-6), interleukin 8 (IL-8), and interleukin 1α (IL-1α) mRNA and proteins levels ($n = 6$; $n = 5$) in primary human limbal epithelial cells (pLECs) 72 h after transfection with control siRNA (blue) or with FOXC1 knockdown siRNA (pink), without or with lipopolysaccharide (LPS) or interleukin 1β (IL-1β) treatment (**A**–**F**). Data are shown as mean ± SD. Data have been tested for normal distribution using Shapiro–Wilk test. Statistical analysis has been performed using two-way ANOVA followed by Tukey test. *p*-values below 0.05 were considered statistically significant. Each data point represents an individual donor. FOXC1 siRNA knockdown downregulated IL-6 mRNA and protein levels in cell culture supernatant without and with LPS or IL-1β compared to siRNA controls ($p \leq 0.011$). In addition, in FOXC1 siRNA knockdown pLECs with IL-1β treatment, IL-6 protein levels were higher than in those without and with LPS treatment ($p \geq 0.002$). IL-6 proteins levels were upregulated in FOXC1 siRNA knockdown pLECs with IL-1β-induced inflammation compared to LPS-induced inflammation ($p = 0.022$), and non-inflammatory conditions ($p = 0.002$). Also, in control siRNA-treated pLECs with IL-1β-induced inflammation, IL-6 was upregulated compared to non-inflammatory conditions ($p = 0.009$) (**A**,**D**). FOXC1 siRNA knockdown downregulated *IL-8* mRNA levels compared to siRNA controls without and with IL-1β treatment ($p \leq 0.029$). Additionally, the

IL-8 mRNA level was upregulated in siRNA controls with IL-1β treatment compared to LPS-induced inflammation ($p = 0.030$) and non-inflammatory conditions ($p = 0.013$). FOXC1 knockdown in pLECs upregulated IL-8 protein levels in cell culture supernatant compared to siRNA controls without inflammatory treatment ($p = 0.045$). Also, in FOXC1 knockdown pLECs with IL-1β treatment, IL-8 protein levels were downregulated compared to non-inflammatory treated pLECs ($p = 0.017$) (**B**,**E**). FOXC1 siRNA knockdown upregulated *IL-1α* mRNA levels in IL-1β-treated pLECs compared to LPS-treated or non-inflammatory conditions ($p \leq 0.011$). Also, *IL-1α* mRNA levels were upregulated in siRNA controls with LPS- or IL-1β-induced inflammation compared to non-inflammatory conditions ($p \leq 0.003$). FOXC1 knockdown upregulated IL-1α protein levels in cell culture supernatant compared to siRNA controls without induced inflammatory treatment ($p = 0.002$), and in LPS-treated pLECs ($p = 0.015$). Additionally, FOXC1 knockdown upregulated IL-1α protein levels in pLECs without inflammatory treatment compared to IL-1β-treated cells ($p = 0.005$) (**C**,**F**).

The mRNA level of pro-inflammatory cytokine interleukin-8 (IL-8), also known as *chemokine C-X-C motif ligand 8* (*CXCL8*), was downregulated following FOXC1 knockdown both without inflammatory stimuli and in IL-1β-treated conditions compared with siRNA controls ($p \leq 0.029$). In contrast, *IL-8* mRNA was upregulated in control siRNA LECs with IL-1β stimulation compared to non-inflammatory conditions ($p = 0.013$) and LPS-induced inflammation ($p = 0.030$). At the protein level, FOXC1 knockdown increased the IL-8 level under non-inflammatory conditions ($p = 0.045$), but IL-8 protein was reduced in IL-1β-treated knockdown cells compared with untreated pLECs ($p = 0.017$) (Figure 3B,E).

In control siRNA pLECs, pro-inflammatory cytokine *interleukin 1α* (*IL-1α*) mRNA was elevated under both LPS and IL-1β treatment compared to untreated controls ($p \leq 0.003$). For IL-1α, in FOXC1 knockdown pLECs, IL-1β stimulation resulted in higher mRNA levels compared with non-inflammatory or LPS-induced conditions ($p \leq 0.011$). IL-1α protein levels were significantly upregulated after FOXC1 knockdown compared with siRNA controls under basal ($p = 0.002$) and LPS-treated ($p = 0.015$) conditions. Interestingly, in FOXC1 knockdown pLECs, IL-1α protein levels were significantly lower in IL-1β-treated cells than in those without inflammatory stimuli ($p = 0.005$) (Figure 3C,F).

2.4. Chemokine Ligand mRNA and Protein Levels in pLECs

The levels of chemokines in the C-C motif ligand family, C-C motif chemokine ligand 2 (CCL2), C-C motif chemokine ligand 1 (CCL1), and C-C motif chemokine ligand 10 (CCL10), are shown in Figure 4A–F. CCL10 is also known as macrophage inflammatory protein-1γ (MIP-γ). FOXC1 siRNA knockdown in pLECs under non-inflammatory conditions (without LPS or IL-1β) significantly upregulated *CCL2* mRNA levels ($p = 0.007$), whereas CCL2 protein levels in the culture supernatant remained unchanged ($p \geq 0.127$) (Figure 4A,D). In contrast, *CXCL1* and *CXCL10* mRNA and protein levels showed no significant differences following FOXC1 knockdown, either under basal or inflammatory conditions ($p \geq 0.525$) (Figure 4B,C,E,F).

2.5. VEGFA, TNF-α and TGF-β mRNA and Proteins Levels in pLECs

The growth factor, vascular endothelial growth factor A (VEGFA), pro-inflammatory chemokine tumor necrosis factor A (TNF-α), and cytokine transforming growth factor β (TGF-β) mRNA and protein levels are shown in Figure 5A–F. FOXC1 siRNA knockdown significantly reduced *VEGFA* mRNA levels compared with siRNA controls under basal ($p = 0.012$), LPS-treated ($p = 0.022$), and IL-1β treatment conditions ($p = 0.002$) (Figure 5A). However, VEGFA protein levels in the culture supernatant were not significantly affected by FOXC1 knockdown under any condition ($p \geq 0.339$) (Figure 5D).

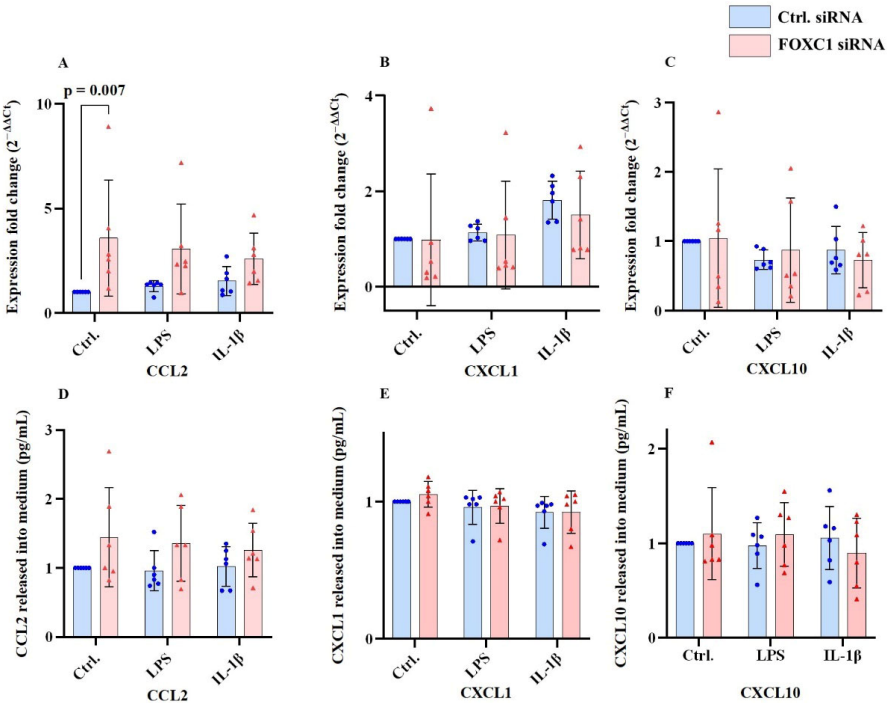

Figure 4. Chemokine ligand 2 (CCL2), chemokine ligand 1 (CXCL1), and chemokine ligand 10 (CXCL10) mRNA and proteins levels (n = 6) in primary human limbal epithelial cells (pLECs) 72 h after transfection with control siRNA (blue) or with FOXC1 knockdown siRNA (pink), without or with lipopolysaccharide (LPS) or interleukin 1β (IL-1β) treatment (**A**–**F**). Data are shown as mean ± SD. Data have been tested for normal distribution using Shapiro–Wilk test. Statistical analysis has been performed using two-way ANOVA followed by Tukey test. p-values below 0.05 were considered statistically significant. Each data point represents an individual donor. FOXC1 siRNA knockdown in pLECs without inflammatory treatment (LPS or IL-1β) upregulated *CCL2* at the mRNA level (p = 0.007) but not at the protein level in the cell culture supernatant ($p \geq 0.127$) (**A**,**D**). *CXCL1*, *CXCL10* mRNA, and protein levels in cell culture supernatant did not change significantly following FOXC1 siRNA knockdown without or with LPS or IL-1β treatment between any of the groups ($p \geq 0.525$) (**B**,**C**,**E**,**F**).

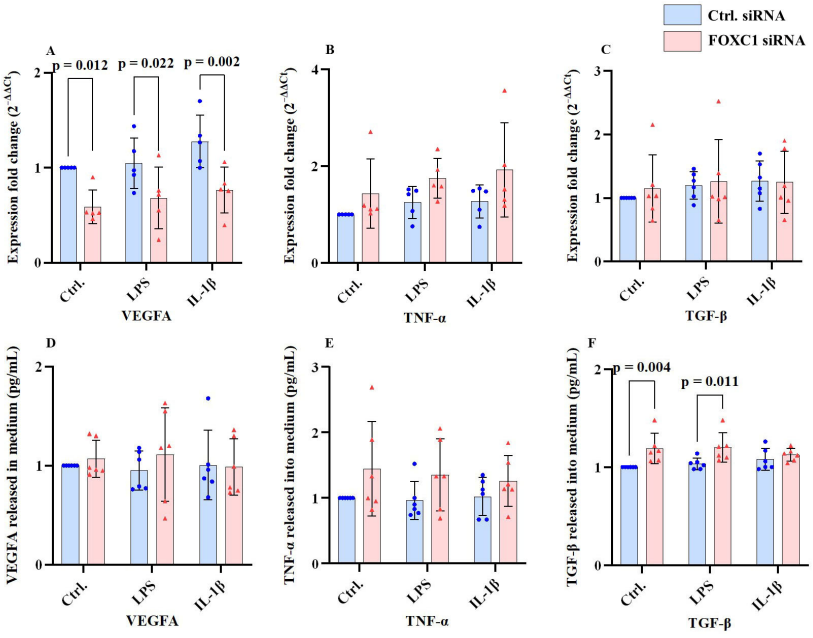

Figure 5. Vascular endothelial growth factor A (VEGFA), tumor necrosis factor α (TNF-α), and transforming growth factor β (TGF-β) mRNA and protein levels (n = 6) in primary human limbal

epithelial cells (pLECs) 72 h after transfection with control siRNA (blue) or with FOXC1 knockdown siRNA (pink), without or with lipopolysaccharide (LPS) or interleukin 1β (IL-1β) treatment (**A**–**F**). Data are shown as mean ± SD. Data have been tested for normal distribution using Shapiro–Wilk test. Statistical analysis has been performed using two-way ANOVA followed by Tukey test. *p*-values below 0.05 were considered statistically significant. Each data point represents an individual donor. FOXC1 siRNA knockdown significantly reduced *VEGFA* mRNA levels compared to siRNA controls under non-inflammatory conditions ($p = 0.012$) as well as after LPS ($p = 0.022$) or IL-1β treatment ($p = 0.002$) (**A**). In contrast, FOXC1 knockdown did not significantly affect VEGFA protein levels in the culture supernatant under any condition, with or without LPS or IL-1β stimulation ($p \geq 0.339$) (**D**). Similarly, FOXC1 knockdown did not alter *TNF-α* mRNA ($p \geq 0.076$) or protein levels ($p \geq 0.086$) in the culture supernatant (**B**,**E**), nor did it affect *TGF-β* mRNA expression ($p \geq 0.544$) (**C**). However, FOXC1 siRNA knockdown led to a significant increase in TGF-β protein levels under non-inflammatory ($p = 0.004$) and LPS-treated conditions ($p = 0.011$) but not following IL-1β stimulation ($p = 0.449$) (**F**).

Similarly, TNF-α mRNA ($p \geq 0.076$) and protein levels ($p \geq 0.086$) remained unchanged between FOXC1 knockdown and control cells (Figure 5B,E), as did *TGF-β* mRNA levels ($p \geq 0.544$) (Figure 5C). In contrast, TGF-β protein levels were significantly upregulated in FOXC1 knockdown LECs under non-inflammatory ($p = 0.004$) and LPS-treated conditions ($p = 0.011$), but not after IL-1β stimulation ($p = 0.449$) (Figure 5F).

2.6. CYP1B1 and PAX6 mRNA and Proteins Levels in pLECs

Figure 6A–F display cytochrome P450 family 1 subfamily B1 (CYP1B1) and paired box 6 (PAX6) mRNA and protein levels. FOXC1 siRNA knockdown significantly reduced *CYP1B1* mRNA levels compared with siRNA controls under basal, LPS-, and IL-1β-treated conditions ($p < 0.001$). In contrast, CYP1B1 protein levels remained unchanged following FOXC1 knockdown in all groups ($p \geq 0.268$) (Figure 6A–C).

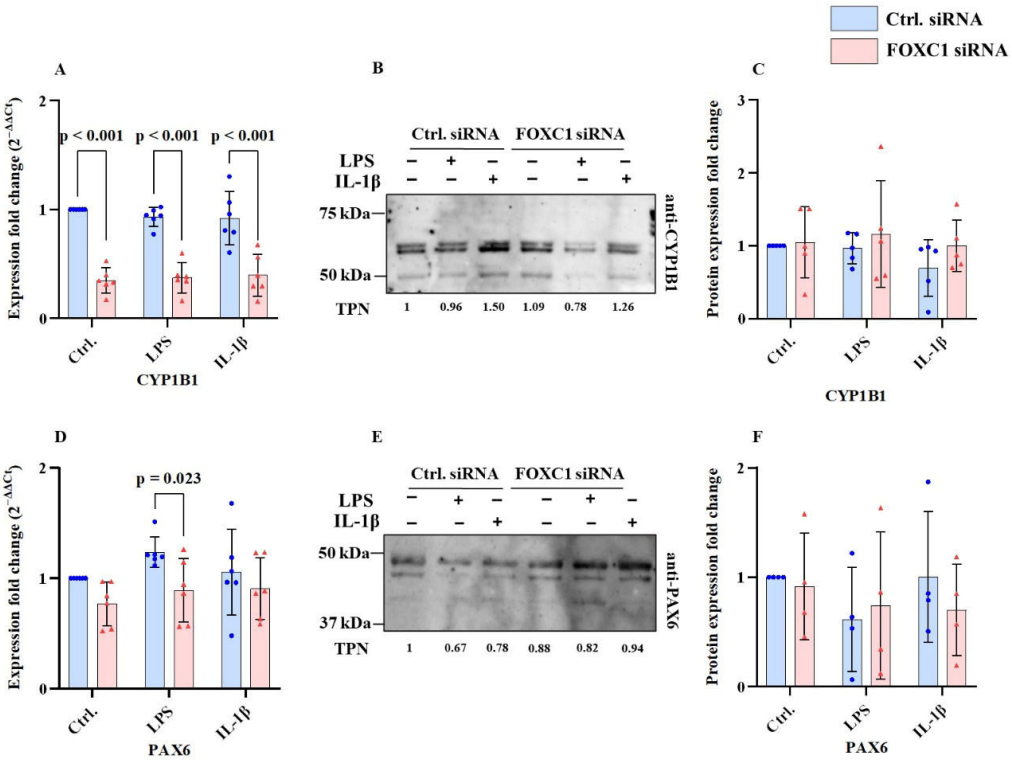

Figure 6. Cytochrome P450 (CYP1B1), and paired box protein 6 (PAX6) mRNA and protein levels ($n = 6$; $n = 5$) in primary human limbal epithelial cells (pLECs) 72 h after transfection with control

siRNA (blue) or with FOXC1 knockdown siRNA (pink), without or with lipopolysaccharide (LPS) or interleukin 1β (IL-1β) treatment (**A**–**F**). Data are shown as mean ± SD. Data have been tested for normal distribution using Shapiro–Wilk test. Statistical analysis has been performed using two-way ANOVA followed by Tukey test. *p*-values below 0.05 were considered statistically significant. Each data point represents an individual donor. FOXC1 siRNA knockdown significantly reduced *CYP1B1* mRNA expression compared to siRNA controls under both non-inflammatory and inflammatory conditions (LPS or IL-1β treatment) ($p < 0.001$). However, CYP1B1 protein levels did not change significantly following FOXC1 knockdown under any condition ($p \geq 0.268$) (**A**–**C**). Similarly, FOXC1 siRNA knockdown resulted in decreased *PAX6* mRNA expression compared to siRNA controls after LPS treatment ($p = 0.023$). In contrast, PAX6 protein levels remained unchanged across all conditions, regardless of inflammatory stimulation (**D**–**F**).

Using LPS treatment, the *PAX6* mRNA level was significantly downregulated in FOXC1 knockdown LECs compared with siRNA controls ($p = 0.023$). However, PAX6 protein levels did not differ significantly between groups, either without or with inflammatory conditions ($p \geq 0.393$) (Figure 6D–F).

2.7. FABP5 and CRABP2 mRNA and Proteins Levels in pLECs

Fatty acid-binding protein 5 (FABP5) and cellular retinoic acid-binding protein 2 (CRABP2) mRNA and protein levels are shown in Figure 7A–G. FOXC1 siRNA knockdown significantly reduced *FABP5* mRNA levels compared with siRNA controls under non-inflammatory conditions ($p < 0.001$). In contrast, in FOXC1 knockdown pLECs, *FABP5* mRNA levels were upregulated following IL-1β treatment compared to untreated cells ($p = 0.001$). FABP5 protein levels remained unchanged across all treatment conditions ($p \geq 0.311$) (Figure 7A–C).

The *CRABP2* mRNA level was downregulated following FOXC1 knockdown under both basal ($p = 0.037$) and IL-1β-treated conditions ($p = 0.003$). In control siRNA-transfected LECs, *CRABP2* mRNA was upregulated after IL-1β stimulation compared to non-inflammatory conditions ($p = 0.013$). At the protein level, CRABP2 was significantly reduced in FOXC1 knockdown cells compared with siRNA controls under non-inflammatory conditions ($p = 0.012$) (Figure 7D–F).

In control siRNA pLECs, the FABP5/CRABP2 protein ratio was higher under basal conditions compared with IL-1β treatment ($p = 0.004$). In addition, in control siRNA pLECS, the FABP5/CRABP2 protein ratio was significantly higher following LPS treatment than after IL-1 β use ($p = 0.026$). An analysis of the FABP5/CRABP2 protein ratio revealed that, in FOXC1 knockdown pLECs, the FABP5/CRABP2 protein ratio was significantly lower under IL-1β-induced inflammation than without inflammatory conditions ($p = 0.006$) (Figure 7G).

2.8. Further Retinoic Acid Signaling Pathway-Related mRNA and Protein Levels in pLECs

Retinoic acid signaling pathway-related mRNA and protein levels are displayed in Figure 8A–L. FOXC1 siRNA knockdown significantly reduced retinol dehydrogenase 10 (*RDH10*) mRNA levels compared with siRNA controls under basal, LPS-, and IL-1β-treated conditions ($p < 0.001$). RDH10 protein levels were also decreased in FOXC1 knockdown pLECs under non-inflammatory conditions ($p = 0.017$) (Figure 8A–C).

Signaling receptor and transporter of retinoic acid (*STRA6*) mRNA levels were also significantly downregulated in FOXC1 knockdown cells compared with siRNA controls under basal ($p = 0.005$), LPS-treated ($p = 0.013$), and IL-1β-treated ($p = 0.006$) conditions. However, STRA6 protein levels were not significantly affected by FOXC1 knockdown in any of the groups ($p \geq 0.114$) (Figure 8D–F).

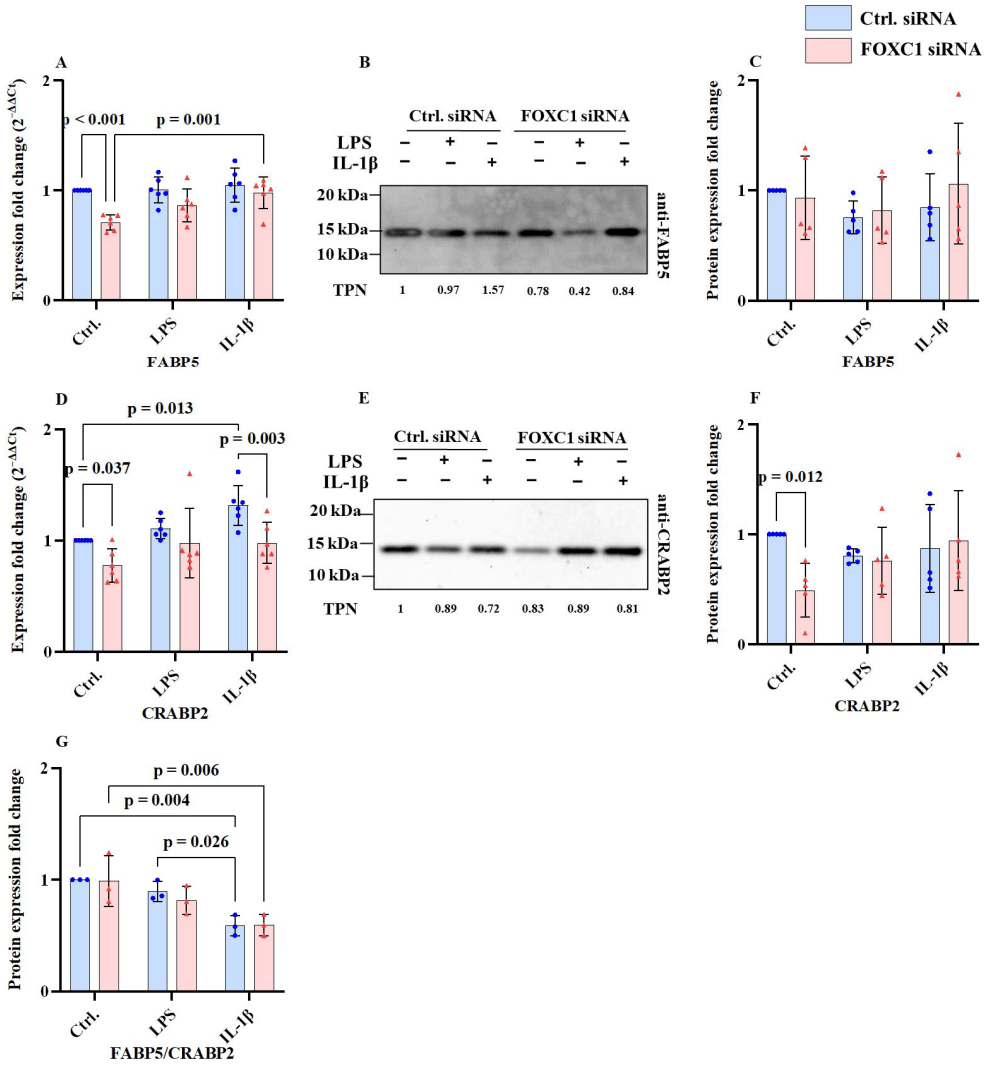

Figure 7. Fatty acid-binding protein 5 (FABP5) and cellular retinoic acid-binding protein 2 (CRABP2) mRNA and protein levels (n = 6; n = 5) in primary human limbal epithelial cells (pLECs) 72 h after transfection with control siRNA (blue) or with FOXC1 knockdown siRNA (pink), without or with lipopolysaccharide (LPS) or interleukin 1β (IL-1β) treatment. FABP5-CRABP2 ratio depicting FABP5-CRABP2 regulatory axis (**A**–**G**). Data are shown as mean ± SD. Data have been tested for normal distribution using Shapiro–Wilk test. Data from *CRABP2* (mRNA) have been tested using Mann–Whitney/Wilcoxon test. Statistical analysis has been performed using two-way ANOVA followed by Tukey test. p-values below 0.05 were considered statistically significant. Each data point represents an individual donor. FOXC1 siRNA knockdown significantly reduced *FABP5* mRNA expression compared to siRNA controls under non-inflammatory conditions ($p < 0.001$). In contrast, *FABP5* mRNA levels were upregulated in FOXC1 knockdown pLECs treated with IL-1β compared to untreated cells ($p = 0.001$). However, FABP5 protein levels did not change significantly following FOXC1 knockdown under any condition ($p \geq 0.311$) (**A**–**C**). Similarly, FOXC1 knockdown downregulated *CRABP2* mRNA expression compared to siRNA controls under both non-inflammatory ($p = 0.037$) and IL-1β-treated ($p = 0.003$) conditions. In siRNA control pLECs, *CRABP2* mRNA was upregulated after IL-1β stimulation compared to non-inflammatory conditions ($p = 0.013$). FOXC1 knockdown also resulted in reduced CRABP2 protein levels compared to siRNA controls under non-inflammatory conditions ($p = 0.012$) (**D**–**F**). The ratio of FABP5:CRABP2 protein levels showed that FOXC1 knockdown decreased the FABP5/CRABP2 axis under IL-1β-induced inflammation compared to siRNA controls ($p = 0.006$). In siRNA control pLECs, the FABP5:CRABP2 ratio was higher under non-inflammatory conditions compared to IL-1β ($p = 0.004$) and LPS treatment ($p = 0.026$) (**G**).

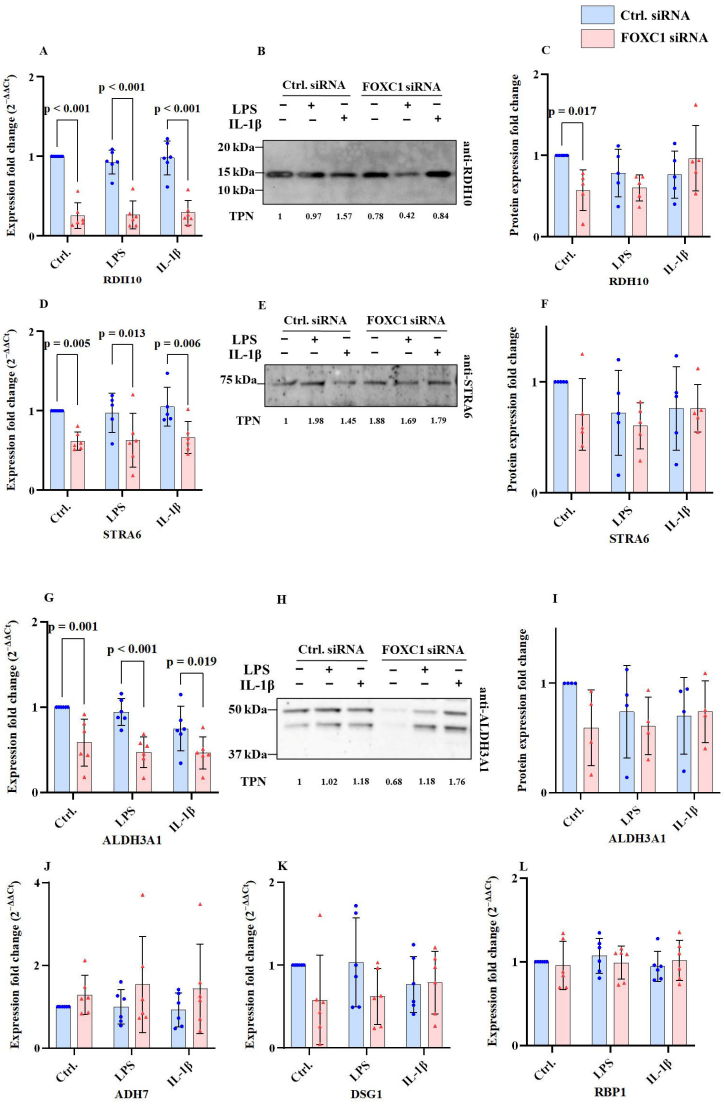

Figure 8. Retinol dehydrogenase 10 (RDH10), signaling receptor and transporter of retinol (STRA6), and aldehyde dehydrogenase 3 family, member A1 (ALDH3A1) mRNA and proteins levels ($n = 6$; $n = 5$); and alcohol dehydrogenase 7 (ADH7), desmoglein 1 (DSG1), and retinol binding protein 1 (*RBP1*) mRNA levels ($n = 6$) in primary human limbal epithelial cells (pLECs) 72 h after transfection with control siRNA (blue) or with FOXC1 knockdown siRNA (pink), without or with lipopolysaccharide (LPS) or interleukin 1β (IL-1β) treatment (**A**–**L**). Data are shown as mean ± SD. Data have been tested for normal distribution using Shapiro–Wilk test. Data from ADH7 have been tested using Mann–Whitney/Wilcoxon test. Statistical analysis has been performed using two-way ANOVA followed by Tukey test. *p*-values below 0.05 were considered statistically significant. Each data point represents an individual donor. FOXC1 siRNA knockdown significantly reduced *RDH10* mRNA expression compared to siRNA controls under both non-inflammatory and inflammatory conditions (LPS or IL-1β treatment) ($p < 0.001$). Correspondingly, RDH10 protein levels were also decreased in FOXC1 knockdown pLECs under non-inflammatory conditions ($p = 0.017$) (**A**–**C**). Similarly, *STRA6* mRNA expression was significantly downregulated in FOXC1 knockdown cells compared to siRNA controls under non-inflammatory ($p = 0.005$), LPS-treated ($p = 0.013$), and IL-1β-treated ($p = 0.006$) conditions. However, STRA6 protein levels were not significantly affected by FOXC1 knockdown under any treatment ($p \geq 0.114$) (**D**–**F**). FOXC1 knockdown also resulted in significantly decreased *ALDH3A1* mRNA expression compared to siRNA controls under non-inflammatory ($p = 0.001$), LPS ($p < 0.001$), and IL-1β ($p = 0.019$) conditions. In contrast, ALDH3A1 protein levels remained unchanged between groups across all treatments ($p \geq 0.078$) (**G**–**I**). No significant changes were observed in ADH7, DSG1, or *RBP1* mRNA expression following FOXC1 knockdown under any condition ($p \geq 0.077$) (**J**–**L**).

Enzyme aldehyde dehydrogenase 3 family member A1 (*ALDH3A1*) mRNA expression was likewise reduced after FOXC1 knockdown compared to siRNA controls under non-inflammatory ($p = 0.001$), LPS ($p < 0.001$), and IL-1β ($p = 0.019$) conditions. In contrast, ALDH3A1 protein levels remained unchanged between all groups ($p \geq 0.078$) (Figure 8G–I).

No significant changes were observed in aldehyde dehydrogenase 7 (*ADH7*), desmoglein-1 (*DSG1*), or retinol-binding protein 1 (*RBP1*) mRNA levels following FOXC1 knockdown under any experimental condition ($p \geq 0.077$) (Figure 8J–L).

2.9. PPARγ, FOSL2, SPINK7, MMP2, MAPK1/ERK2, MAPK3 and Mki67 mRNA Levels in pLECs

The mRNA levels of peroxisome proliferator-activated receptor gamma (*PPARγ*), nuclear factor kappa-light-chain-enhancer of activated B cells (*NF-κB*), serine peptidase inhibitor kazal type 7 (*SPINK7*), matrix metalloproteinase 2 (*MMP2*), mitogen-activated protein kinase 3/extracellular signal-regulated kinase 2 (*MAPK1/ERK2*), and mitogen-activated protein kinase 3 (*MAPK3*) showed no significant differences following FOXC1 siRNA knockdown across any group or treatment condition ($p \geq 0.346$) (Figure 9A–H). Nevertheless, FOXC1 siRNA knockdown resulted in a significant reduction in fos-like antigen 2 (*FOSL2*) mRNA levels in pLECs under non-inflammatory conditions compared to siRNA controls ($p = 0.048$), while no significant differences were observed under inflammatory treatments ($p \geq 0.080$) (Figure 9C). In contrast, FOXC1 siRNA knockdown significantly increased marker protein Ki-67 (*MKi67*) mRNA levels in pLECs under non-inflammatory conditions compared to siRNA controls ($p = 0.006$), with no statistically significant changes detected under inflammatory conditions ($p \geq 0.117$) (Figure 9H).

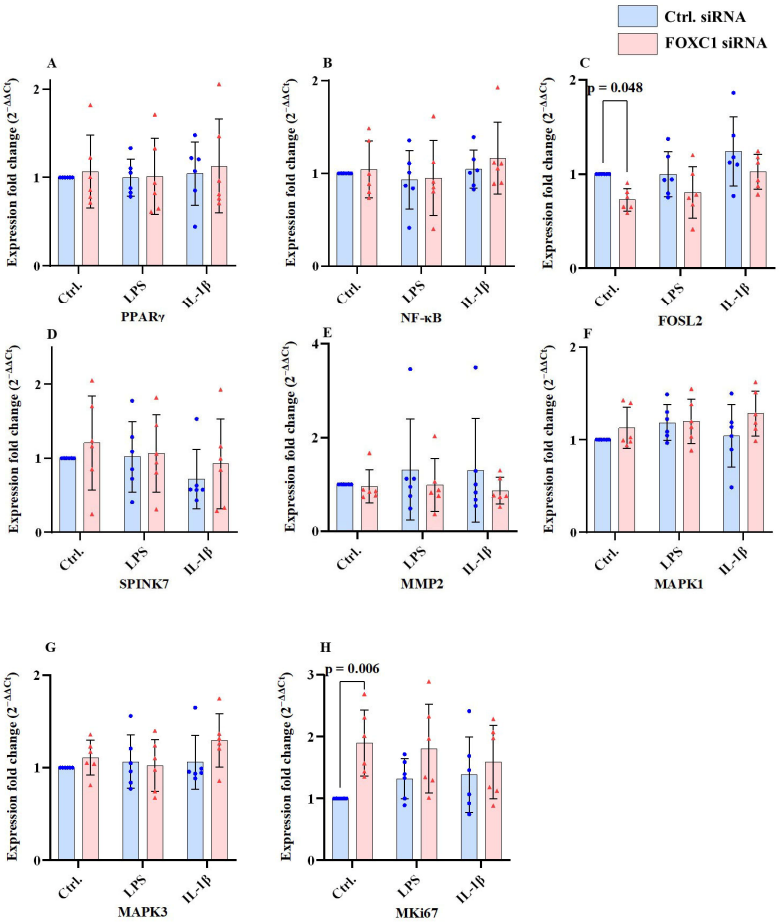

Figure 9. Peroxisome proliferator-activated receptor gamma (PPARγ), nuclear factor kappa-light-chain-enhancer of activated B cells (NF-κB), fos-like antigen 2 (FOSL2), serine peptidase inhibitor

kazal type 7 (SPINK7), matrix metalloproteinase 2 (MMP2), mitogen-activated protein kinase 3/extracellular signal-regulated kinase 2 (MAPK1/ERK2), mitogen-activated protein kinase 3 (MAPK3), and proliferation marker protein Ki-67 (*Mki67*) mRNA levels (n = 6) in primary human limbal epithelial cells (pLECs) 72 h after transfection with control siRNA (blue) or with FOXC1 knockdown siRNA (pink), without or with lipopolysaccharide (LPS) or interleukin 1β (IL-1β) treatment (**A**–**H**). Data are shown as mean ± SD. Data have been tested for normal distribution using Shapiro–Wilk test. Data from FOSL2 have been tested using Mann–Whitney/Wilcoxon test. Statistical analysis has been performed using two-way ANOVA followed by Tukey test. p-values below 0.05 were considered statistically significant. Each data point represents an individual donor. *PPARγ*, *NF-κB*, *SPINK7*, *MMP2*, *MAPK1/ERK2*, and *MAPK3* mRNA expression levels were not significantly affected by FOXC1 siRNA knockdown under any condition or treatment ($p \geq 0.346$) (**A**,**B**,**D**–**G**). FOXC1 knockdown significantly reduced *FOSL2* mRNA expression in pLECs under non-inflammatory conditions compared to siRNA controls ($p = 0.048$), while no significant differences were observed under inflammatory treatments ($p \geq 0.080$) (**C**). In contrast, FOXC1 knockdown significantly increased *MKi67* mRNA expression in pLECs under non-inflammatory conditions compared to siRNA controls ($p = 0.006$), with no statistically significant changes detected under inflammatory conditions ($p \geq 0.117$) (**H**).

3. Discussion

3.1. FOXC1 Transcriptional Efficiency, Protein Turnover Rate and Stability and Downstream Pathways

In our study, despite the efficient FOXC1 siRNA-mediated knockdown in pLECs, we did not observe a corresponding significant reduction in FOXC1 protein levels within the 72 h period assessed through a densitometric analysis of Western blots. To better understand this discrepancy between mRNA and protein levels, we extended our analyses to 48, 72, and 96 h time points. These experiments suggested that FOXC1 protein turnover occurs more slowly than transcriptional suppression, indicating a possible delay between mRNA downregulation and detectable protein loss. Nevertheless, we also did not observe FOXC1 protein level downregulation at the further examined time points.

Interestingly, FOXC1 appears to exert a broad regulatory influence over multiple downstream pathways, as reflected by the altered expression of other key transcription factors such as FOSL2 and PAX6, both of which play essential roles in epithelial homeostasis and inflammation [1,4]. Furthermore, the concurrent downregulation of both mRNA and protein levels of CRABP2 and RDH10 suggests a direct role for FOXC1 in controlling components of retinoic acid signaling. Changes in the proliferation marker MKi67 and the discordant expression patterns between mRNA and protein levels of several FOXC1-regulated targets—such as TGF-β, interleukins, and chemokines—underscore the complexity of post-transcriptional and post-translational mechanisms that modulate protein abundance independently of transcriptional activity. These findings emphasize the importance of considering temporal and regulatory dynamics when interpreting FOXC1-related molecular changes (Figure 10). This phenomenon has been well characterized in large-scale system biology studies. Schwanhäuser et al. [25] performed a landmark analysis combining the parallel metabolic pulse labeling of RNA and proteins across diverse mammalian cell types, demonstrating that protein levels are considerably more dynamic and less tightly correlated with mRNA abundance. Although mRNA and protein levels are generally proportional, the correlation remains in some cases weak, suggesting that post-transcriptional regulation, translation efficiency, and protein degradation rates collectively determine the final protein abundance. Subsequent studies confirmed that, in steady-state tissues, protein stability is often favored, such that even substantial fluctuations in mRNA levels do not necessarily lead to proportional changes at the protein level [26,27]. In non-proliferating tissues, this decoupling is particularly evident, as cellular protein abundance depends heavily on differentiation state and post-translational control mechanisms [26]. Reduced mRNA expression

does not always equate to diminished protein synthesis, since translation efficiency and protein stability may compensate for transcriptional changes [25–27].

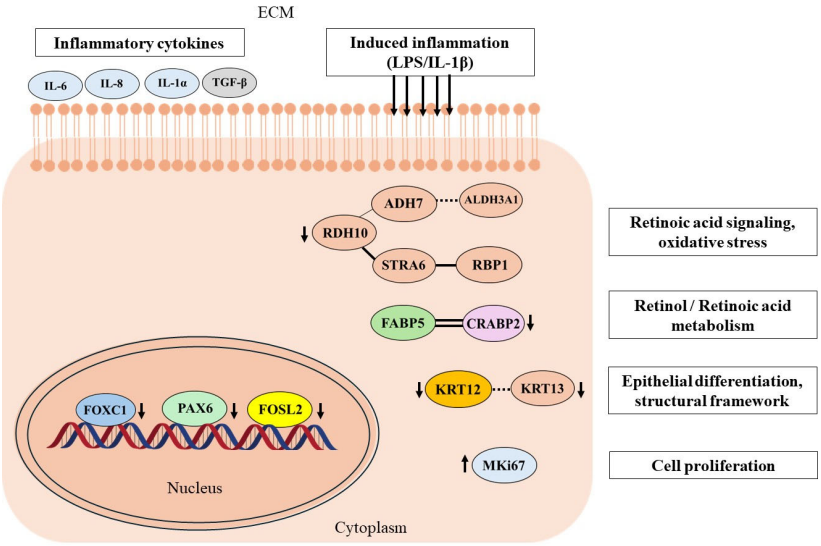

Figure 10. The effects of FOXC1 siRNA-mediated knockdown in primary limbal epithelial cells (pLECs) on retinol metabolism, retinoic acid signaling, epithelial differentiation, cellular proliferation, and inflammatory cytokine secretion. The depicted interactions are derived from data generated in this study and integrated with information from the STRING and KEGG databases. ADH7: aldehyde dehydrogenase 7; ALDH3A1: enzyme aldehyde dehydrogenase 3 family member A1; CRABP2: cellular retinoic acid-binding protein 2; FOSL2: fos-like antigen 2; IL-6: interleukin-6; IL-8: interleukin-8; IL-1α: interleukin-1α; KRT12: cytokeratin 12; KRT13: cytokeratin 13; MKi67: marker protein Ki-67; FABP5: fatty acid-binding protein 5; PAX6: paired box 6; RBP1: retinol-binding protein 1; RDH10: retinol dehydrogenase 10; STRA6: signaling receptor and transporter of retinoic acid; TGF-β: transforming growth factor β.

In line with these observations, our results indicate that FOXC1 mRNA and protein levels are not always fully aligned in pLECs, suggesting the involvement of complex post-transcriptional and post-translational regulatory mechanisms. Factors contributing to this discrepancy may include functional or structural protein modifications, such as changes in phosphorylation status, which can occur independently of transcription or translation. In addition, regulatory effects mediated by non-coding RNAs may influence mRNA stability and translational efficiency, thereby modulating protein output. To further elucidate these regulatory processes, future studies employing advanced high-throughput approaches may be particularly informative. Proteomic analyses [28] could provide insights into protein stability, post-translational modifications, and interaction networks, while single-cell RNA sequencing [29] may help resolve cell-type-specific regulatory heterogeneity. Together, these complementary approaches may contribute to a more comprehensive understanding of FOXC1 regulation at both the transcriptional and post-transcriptional levels.

3.2. FOXC1 as a Regulator of Angiogenic Pathways and Chemokine and Cytokine Signaling

In the angiogenetically privileged environment of the cornea, a delicate equilibrium between pro- and anti-angiogenic factors is essential for maintaining avascularity and transparency. Pathological angiogenesis, characterized by neovascularization extending from the limbus into adjacent corneal tissue, disrupts this balance and has been investigated in murine models, where FOXC1 has emerged as a critical regulator of hematopoietic progenitor niche formation [11,13,30,31]. The presence of soluble VEGF receptors provides a potent anti-angiogenic mechanism that contributes to corneal vascular privilege [13,18,31]. Moreover, FOXC1 enhances the expression of inflammation-related cytokines (CCL2,

NF-κB) [32,33]. In our data, we observed a global downregulation of VEGFA at the transcriptional level, but not at the protein level, suggesting a potential translational blockade or spatially restricted expression of VEGFA in limbal epithelial cells. Under basal conditions, FOXC1 knockdown increased *CCL2* mRNA levels, yet protein secretion remained unaltered. Similarly, CXCL1, CXCL10, and VEGFA showed no significant protein-level changes despite some transcriptional alterations. These findings suggest that FOXC1 primarily modulates the transcriptional priming of chemokine and growth factor genes, highlighting the importance of transcription–protein discordance in regulating pLEC inflammatory response. It is possible that FOXC1 influences cytokine processing or stability, or that compensatory inflammatory pathways are activated upon FOXC1 depletion. Given that IL-1α mediates epithelial injury responses and immune cell recruitment [34], FOXC1-deficient pLECs may upregulate IL-1α signaling to counterbalance dampened IL-6/IL-8 activity and preserve immune vigilance. Collectively, these data support a model in which FOXC1 maintains an anti-inflammatory, immune-quiescent state in pLECs, restraining excessive pro-inflammatory activation under homeostatic conditions.

3.3. Implications of FOXC1 mRNA Silencing on pLEC Function, Differentiation and Corneal Homeostasis—Via TGF-β Signaling and Epithelial Differentiation Markers

FOXC1 functions as a downstream effector of several major epithelial-to-mesenchymal transition (EMT) signaling pathways, including TGF-β, Smad2/3, Snail, and Twist. This mechanistic positioning may explain why transcriptional changes were modest, yet alterations at the protein level were evident for TGF-β. In HeLa cell lines with homoallelic FOXC1 deletion, ectopic FOXC1 expression was shown to restore TGF-β-mediated cell cycle inhibition by arresting cells in the G0/G1 phase [33,35–37]. In a previous study using limbal stromal cells or limbal fibroblasts derived from aniridia and healthy donors, an exposure to high glucose resulted in the downregulation of TGF-β, Smad2/3, and NF-κB transcripts, accompanied by increased oxidative stress [33]. The multifunctional cytokine TGF-β is well established as a master regulator of wound healing, fibrosis, EMT, extracellular matrix deposition, and cell proliferation and differentiation. In the current study, we observed elevated TGF-β protein levels in FOXC1-deficient pLECs under both basal and LPS-induced inflammatory conditions. This upregulation may signify a phenotypic shift toward fibrotic repair processes and pathological ocular remodeling. These findings further support a potential positive feedback loop in which secreted TGF-β modulates FOXC1 expression, thereby potentially influencing apoptotic regulation [36,37]. Additionally, LPS-stimulated cells activate immune signaling cascades that interact with macrophages, enhancing TGF-β secretion and secondary cytokine production [36,38].

Keratin expression in LECs is known to be retinoic acid metabolism-sensitive [38–40]. The KRT3/KRT12 heterodimer, which defines corneal epithelial identity, is disrupted in several ocular disorders including aniridia, Meesmann corneal dystrophy (MECD), and corneal ulcerations [41]. Although FOXC1 is not a universal regulator of epithelial keratin genes, it plays a targeted role in safeguarding corneal epithelial identity. Consistent with our findings, a seminal ChIP-sequencing study by Li et al. [8] identified FOXC1 as a transcriptional regulator of corneal lineage commitment. Transcriptomic analysis further demonstrated that FOXC1 knockdown in corneal epithelial cells downregulated 468 genes, including corneal epithelial markers KRT3 and KRT12, while upregulating epidermal keratins KRT1 and KRT10, indicating a lineage identity switch. FOXC1 dysregulation also perturbs PAX6 expression, further compromising limbal stem cell lineage stability.

In our dataset, KRT12 and KRT13 were downregulated under basal and IL-1β-induced inflammatory conditions, respectively. These findings suggest that these keratins act downstream of FOXC1 and may be influenced by retinoid or cytokine-mediated regulatory networks. Notably, KRT13, a conjunctival epithelial marker implicated in enhanced stem-

ness and metastasis via c-Myc signaling in breast cancer [20], was reduced following FOXC1 knockdown. In contrast, KRT19, a progenitor stem cell marker expressed in the LSC niche, and KRT3, a mature corneal epithelial marker, did not exhibit significant transcriptional variation. This pattern underscores the specific and selective regulatory influence of FOXC1 on keratin gene networks. Together, these observations reveal that FOXC1 orchestrates a finely tuned balance between TGF-β-mediated EMT, keratin expression, and inflammatory signaling, thereby preserving corneal epithelial identity and preventing pathological remodeling. Alterations in FOXC1 expression disrupt this balance, predisposing the ocular surface to fibrosis, lineage instability, and inflammatory degeneration [36].

Previous studies have demonstrated that the presence of inflammatory mediators is associated with disrupted epithelial differentiation and a pronounced reduction in LSC populations. In parallel, cellular proliferative capacity and stemness-related characteristics are significantly impaired [42,43]. These findings suggest that intense inflammatory conditions can indirectly compromise LSC function and viability without necessarily causing immediate structural damage to the limbal niche. Instead, persistent inflammation appears to induce maladaptive changes in the limbal microenvironment, leading to aberrant epithelial differentiation and promoting pathological processes such as neovascularization originating from the limbal region [42,43].

3.4. Understanding Retinoic Acid Metabolic Pathway and Its Link to Limbal Epithelium via FOXC1 siRNA Knockdown

At the time of this study, there have been no direct reports describing the mechanistic relationship between FOXC1 and RA metabolism or signaling in pLECs. It is noteworthy that the anterior segment of the eye, along with the forebrain and meninges, originates from the neural crest during embryonic development. FOXC1 plays a crucial developmental role in this context, as FOXC1 mutant mice exhibit a reduced or absent expression of RDH10 and RALDH2, key enzymes responsible for RA biosynthesis from retinal [44,45]. Consequently, FOXC1 deficiency disrupts RA signaling during neurogenesis, affecting Notch- and SOX2-dependent self-renewal pathways [44]. Altered FOXC1 expression or dosage is known to underlie Axenfeld–Rieger syndrome and other neural crest-related malformations. These defects have dual ramifications: (i) central nervous system abnormalities and (ii) altered RA signaling derived from the meninges and anterior ocular structures.

Given this developmental linkage, we investigated whether FOXC1 knockdown would influence the expression of genes involved in RA metabolism in pLECs. Notably, patients with FOXC1 haploinsufficiency—similar to ARS—often present with corneal neovascularization, further implicating FOXC1 in anterior segment homeostasis.

A central finding of our study is that FOXC1 silencing in pLECs led to the downregulation of RA pathway genes *RDH10*, *CRABP2*, and *ALDH3A1*, accompanied by decreased protein levels of RDH10 and CRABP2. Several studies have established RA signaling as a cornerstone of corneal epithelial differentiation, immune regulation, and stem cell maintenance, reinforcing the functional importance of these observations [44,46]. Interestingly, other RA metabolic genes, such as *RBP1* and *ADH7*, remained unchanged, indicating that FOXC1 exerts a selective and targeted effect on specific RA pathway components rather than inducing a global suppression of RA metabolism. We therefore propose that impaired RA signaling resulting from FOXC1 dysregulation may compromise epithelial barrier integrity and contribute to pathological remodeling, consistent with FOXC1's established roles in ocular development and disease [11,18,19].

Furthermore, the observed alteration in the FABP5–CRABP2 axis provides additional insight into the metabolic shift within the RA network. These two binding proteins direct RA toward distinct downstream fates: FABP5 promotes proliferative, pro-survival signaling through PPARβ/δ, whereas CRABP2 mediates differentiation and apoptotic responses via

RAR activation [44,46]. In our study, the FABP5/CRABP2 ratio decreased, particularly under IL-1β-induced inflammatory conditions following FOXC1 knockdown, suggesting a functional bias toward differentiation/apoptosis-resistant phenotypes. This finding is consistent with upregulated MKi67 expression, reflecting enhanced cellular proliferation. Notably, FOXC1 has been recognized as an oncogenic marker across multiple cancer types, while CRABP2 has been implicated in apoptotic regulation and epigenetic homeostasis in corneal epithelial cells [46,47]. In line with Tang et al. [48], elevated CRABP2 expression has been shown to mitigate DNA methylation-associated mitochondrial apoptosis, suggesting a complex interplay between FOXC1, RA signaling, and cell survival mechanisms in maintaining limbal epithelial equilibrium. Collectively, these findings establish a novel connection between FOXC1 and retinoic acid metabolism in pLECs, positioning FOXC1 as a potential upstream regulator of RA-dependent epithelial homeostasis. The data highlight how the disruption of FOXC1 may lead to aberrant RA flux, altered proliferative–differentiation balance, and impaired regenerative capacity at the limbal niche.

4. Materials and Methods

4.1. Ethical Considerations

The use of donor corneoscleral buttons and corneoscleral rim tissue in our experiments was approved by the Ethical Committee of Saarland/Germany (No. 162/23). All procedures involving human donor tissue were conducted in accordance with the principles of the Declaration of Helsinki. Written informed consent was obtained from all donors. De-identified donor information is summarized in Table 1.

Table 1. Demographic information (gender and age) of de-identified healthy corneal donors used in this study has been tabulated below. The data are based on information provided by the Lions Cornea Bank Saar-Lor-Lux, Trier/Westpfalz & Klaus Faber Centre.

Donors	Gender (42.85% Male)	Age (Years) 76.16 ± 6.87 (67–92)
Donor 1	Male	67
Donor 2	Male	68
Donor 3	Female	72
Donor 4	Male	77
Donor 5	Female	81
Donor 6	Female	92
Donor 7	Female	Unknown

4.2. Cell Culture

pLEC cultures were generated following previously published protocols [40,41,49,50]. Limbal tissue was collected from healthy corneal donors using a 1.5 mm biopsy punch (PFM Medical AG, Köln, Germany). The obtained tissue samples were incubated in 700 µL of collagenase A solution (4 mg/mL; Roche Pharma AG, Basel, Switzerland) for 24 h at 37 °C in a humidified atmosphere containing 5% CO_2 to enable enzymatic dissociation. Following digestion, the cell suspension was centrifuged at 0.2× *g* for 5 min to separate epithelial cells from residual tissue fragments and enzyme-containing medium. The resulting cell pellet was then resuspended in 800 µL of supplemented Keratinocyte Growth Medium 3 (KGM3; PromoCell GmbH, Heidelberg, Germany) containing 0.06 mM $CaCl_2$ and the recommended supplement mixture. For subsequent experiments, pLECs were plated in six-well, clear-bottom culture plates (Greiner Bio-One GmbH, Frickenhausen, Germany) and cultured under standard conditions.

siRNA Transfection of pLECs and Inflammatory Treatment

pLECs at passages one or two were seeded into six-well culture plates and transfected with siRNA at approximately 60% confluency. Control cells were transfected with 150 pmol of non-targeting control siRNA (catalog No. #4390843, Silencer™ Select Negative Control, Thermo Fisher Scientific, Waltham, Massachussets (MA), USA). For FOXC1 silencing, cells were transfected with 150 pmol of FOXC1-specific siRNA (5′→3′: sense, GAACGGGAAUAGUAGCUGUtt; antisense, ACAGCUACUAUUCCCGUUCac; catalog No. #4392420, Silencer™ Select FOXC1, Thermo Fisher Scientific, Waltham, Massachussets (MA), USA). The FOXC1 siRNA targets the coding sequence of human FOXC1 mRNA (RefSeq NM_001453). The antisense strand of the siRNA serves as the guide strand and specifically aligns to the *FOXC1* mRNA sequence. The target region (5′-ACAGCTACTATTCCCGTTC-3′; DNA format, no overhang) was verified using the UCSC Genome Browser (GRCh38/hg38) to confirm its specificity. The corresponding mRNA target location is also reported in Table 2. Transfection mixtures were prepared as previously described by Kundu et al. [50]. Briefly, 150 pmol of siRNA was diluted in 250 µL of Opti-MEM™ (1×) supplemented with GlutaMAX™ (Gibco, El Centro, California (CA), USA). In parallel, 7.5 µL of Lipofectamine™ 2000 Transfection Reagent (Thermo Fisher Scientific, Waltham, Massachussets (MA), USA) was diluted in 250 µL of Opti-MEM™ with GlutaMAX™ and incubated for 5 min. The diluted siRNA and Lipofectamine solutions were then combined and incubated for 20 min to allow complex formation. A total volume of 509 µL of the transfection complex was added to each well, together with 2 mL of supplemented KGM3 medium. After 24 h, the transfection medium was replaced with fresh supplemented KGM3. Forty-eight hours after transfection, inflammatory stimulation was induced by treating cells with lipopolysaccharide (LPS; Sigma-Aldrich, Rehovot, Central District, Israel) or interleukin-1β (IL-1β; PeproTech, Cranbury, New Jersey (NJ), USA). For LPS treatment, 2.5 µL was added to achieve a final concentration of 2 µg/mL per well, and, for IL-1β treatment, 0.25 µL was added to reach a final concentration of 1 ng/mL per well (total volume 2.5 mL per well). The experimental groups included: (i) control siRNA or FOXC1 siRNA without inflammatory stimulation; (ii) control siRNA or FOXC1 siRNA with LPS treatment (2 µg/mL); and (iii) control siRNA or FOXC1 siRNA with IL-1β treatment (1 ng/mL). Culture supernatants from all treatment conditions were collected for subsequent ELISA analysis. Cell lysates were prepared 72 h after transfection using SKP buffer provided in the RNA/DNA/Protein Purification Plus Micro Kit (Norgen, Thorold, ON, Canada; catalog No. 47700).

4.3. RNA/Protein Extraction and cDNA Synthesis

Cell lysates were processed for simultaneous isolation of RNA and protein using the RNA/DNA/Protein Purification Plus Micro Kit (Norgen, Thorold, ON, Canada; catalog No. 47700) in accordance with the manufacturer's instructions. Using this Kit, genomic DNA was removed at the initial step, followed by dedicated procedures for RNA purification. RNA concentration was determined using UV/VIS spectrophotometry (ScanDrop, AnalyticJena, Jena, Germany). Protein concentrations were quantified using a standardized Bradford assay (Sigma-Aldrich GmbH, West Springfield, Massachussets (MA), USA) with a spectrophotometric plate reader (Infinite50, TECAN, Zurich, Switzerland).

Complementary DNA (cDNA) was synthesized using the OneTaq RT-PCR Kit (New England Biolabs, Frankfurt am Main, Germany). For each reaction, 1000 ng of total RNA was reverse transcribed using the M-MuLV enzyme mix and oligo(dT) primers provided in the kit. The total reaction volume was 20 µL. Prior to qRT-PCR analysis, 30 µL of nuclease-free water was added to each tube.

Table 2. Information of QuantiTect™ primer pairs used for SYBR-Green-based qRT-PCR, Qiagen (Venlo, The Netherlands).

Target mRNA Transcript with Transcript ID (Source: NCBI)	Catalog No.	Amplicon Size (bp)
ADH7: NM_000673	QT00000217	87 bp
ALDH3A1: NM_000691	QT0240193	121 bp
CCL2: NM_002982	QT00212730	60 bp
CRABP2: NM_001199723	QT00063434	140 bp
CXCL1: NM_001511	QT00199752	120 bp
CXCL10: NM_001565	QT01003065	129 bp
CYP1B1: NM_000104	QT00209496	114 bp
DSG1: NM_001942	QT00001617	96 bp
FABP5: NM_001444	QT00225561	97 bp
FOSL2: NM_005253, XM_005264231, XM_006711976, XM_006711977	QT01000881	126 bp, 177 bp, 229 bp
FOXC1: NM_001453	QT00217161	109 bp
IL-1α: NM_000575	QT00001127	74 bp
IL-6: NM_000600, XM_005249745	QT00083720	107 bp
IL-8: NM_000584	QT00000322	102 bp
KRT3: NM_057088, XM_006719393, XM_005268859, XM_006719392	QT00050365	118 bp
KRT12: NM_000223	QT00011949	104 bp
KRT13: NM_002274, NM_153490	QT00068747	60 bp
KRT19: NM_002276	QT00081137	117 bp
MAPK1: NM_002745, NM_138957	QT00065933	118 bp
MAPK3: NM_001109891, NM_002746	QT02589314	180 bp
MKi67: NM_001145966, NM_002417, XM_006717864	QT00014203	86 bp
MMP2: NM_004530	QT02395778	95 bp
NFkβ: (RELA 2): NM_001243984, NM_001243985, NM_001145138, NM_021975	QT02324308	136 bp
PAX6: NM_000280, NM_001127612, NM_001604, NM_001258462, NM_001258463, NM_001258464, NM_001258465	QT00071169	113 bp
PPARγ: NM_005037, NM_015869, NM_138711, NM_138712, XM_006713208	QT00029841	113 bp
RBP1: NM_002899, NM_001130992, NM_001130993	QT01850296	126 bp
RDH10: NM_172037	QT00029176	107 bp
SPINK7: NM_032566	QT00039585	126 bp
STRA6: NM_001142618, NM_022369, NM_001142617, NM_001199042, NM_001142619, NM_001199041, NM_001199040	QT00006748	74 bp
TBP: NM_001172085, NM_003194	QT00000721	132 bp
TNF-α: NM_000594	QT00029162	98 bp
TGF-β: NM_000594	QT00029162	98 bp
VEGA: NM_001025366, NM_001025367, NM_001025368, NM_001033756, NM_001171623, NM_001171624, NM_001171625, NM_001171626, NM_001171629, NM_003376, NM_001287044	QT01010184	150 bp 204 bp, 222 bp, 273 bp

4.4. Reverse Transcription Quantitative Real-Time Polymerase Chain Reaction (qRT-PCR)

For each qRT-PCR reaction, the following reagents were added to each well of a 96-well plate (MicroAmp™ Optical Reaction Plate, Applied Biosystems, Owings Mills, Maryland (MD), USA): 1 µL cDNA, 1 µL primer, 3 µL nuclease-free water, and 5 µL ACEq DNA SYBR Green Master Mix (Vazyme Biotech, Nanjing, China). All experiments were performed in duplicate using a QuantStudio thermocycler (Thermo Fisher Scientific, Waltham, Massachusetts (MA), USA). The Qiagen QuantiTect™ primers (Qiagen, Venlo,

The Netherlands) used for qPCR are listed in Table 2. TATA binding protein (*TBP*) was used as a reference gene. The amplification conditions for all transcripts were as follows: initial denaturation at 95 °C for 5 min, denaturation at 95 °C for 10 s and primer annealing at 60 °C for 30 s. This was repeated for 40 cycles. Only runs with Ct values within the expected range were considered acceptable. The relative expression was normalized to the *TBP* reference gene expression. Ct and ΔΔCt values were calculated for each target gene compared to controls (control siRNA, no treatment) using QuantStudio™ design and analysis software version 14.3, as described by Livak and Schmittgen [51]. Data analysis and expression fold-changes ($2^{-\Delta\Delta Ct}$ values) were calculated using Microsoft Excel. Using the TBP as the housekeeping gene, acceptable reactions were defined by Ct values within the range of $18 \leq Ct \leq 24$. When the Ct value for TBP exceeded 24, or when a gene known to be expressed within a specific range showed unexpectedly high Ct values, this was considered indicative of suboptimal cDNA quality, and the corresponding data were excluded. For target genes, Ct values between 30 and 32 were considered indicative of low expression and were accepted only when supported by prior knowledge, such as for desmoglein 1 (DSG1), which is known to exhibit higher Ct values. In addition, melting curve analysis consistently showed a single, narrow peak, indicating specific primer binding and the absence of non-specific amplification products. RNA integrity was also regularly verified using agarose gel electrophoresis, which revealed a single, distinct band, confirming high RNA quality.

4.5. Western Blot Analysis

For SDS–PAGE analysis, 15 µg of total protein from each lysate was combined with 5 µL of Laemmli sample buffer and heated at 95 °C for 5 min to achieve complete denaturation. The prepared samples, along with the All-Blue Precision Plus Protein™ Standard (Bio-Rad Laboratories, Munich, Germany), were separated through electrophoresis on 4–12% NuPAGE™ Bis-Tris gels (Invitrogen, Waltham, Massachussets (MA), USA) at 80–100 V. Protein separation was verified using molecular weight markers ranging from 10 to 250 kDa. Following electrophoresis, proteins were transferred to nitrocellulose membranes using a semi-dry blotting system (Trans-Blot Turbo Transfer System, Bio-Rad, Hercules, CA, USA) at 25 V and 1.3 A for 7 min. After transfer, membranes were briefly rinsed with distilled water and stained with No-Stain Protein Labeling Reagent (Invitrogen, Carlsbad, California (CA), USA) to allow total protein normalization (TPN). The membranes were then washed with Froxx Wash Buffer (BioFroxx GmbH, Einhausen, Germany) for 5 min and incubated with the corresponding primary antibodies (listed in Table 3) diluted in Western blot Froxx buffer (BioFroxx GmbH, Einhausen, Germany), which provides combined blocking and antibody incubation solutions. Protein signals were detected using Pierce™ ECL Western Blotting Substrate (Thermo Fisher Scientific, Waltham, MA, USA) and captured with the iBright™ 1500 Imaging System (Thermo Fisher Scientific, Waltham, Massachussets (MA), USA) using universal acquisition settings. Densitometric analysis was performed using iBright™ Analysis Software, version 5.4.0 (Invitrogen, Carlsbad, California (CA), USA).

Table 3. List of primary antibodies used in Western blot and immunoblotting analysis.

Antibody	Source	Molecular Weight (kDa)	Catalog No./Manufacturer	Dilution
ALDH3A1	Rabbit, polyclonal	48 kDa	15578-1-AP, Proteintech, Rosemont, Illinois (IL), USA	1:3000
CRABP2	Mouse, monoclonal	14 kDa	10225-1-AP, Proteintech, Rosemont, Illinois (IL), USA	1:2500

Table 3. *Cont.*

Antibody	Source	Molecular Weight (kDa)	Catalog No./Manufacturer	Dilution
CYP1B1	Rabbit, polyclonal	61 kDa	18505-1-AP, Proteintech, Rosemont, Illinois (IL), USA	1:250
FABP5	Rabbit, polyclonal	15 kDa	12348-1-AP, Proteintech, Rosemont, Illinois (IL), USA	1:1000
FOSL2	Mouse, monoclonal	50 kDa	TA809660S, OriGene Technologies, Rockville, Maryland (MD), USA	1:2000
(i) FOXC1	Rabbit, polyclonal	72 kDa	30082-1-AP, Proteintech, Rosemont, Illinois (IL), USA	1:500
(ii) FOXC1	Mouse, monoclonal	55 kDa	MAB6329-SP, R&D Biotechne, Minneapolis, Minnesota (MN), USA	1:500
KRT12	Mouse, monoclonal	54 kDa	sc-515882, Santa Cruz Biotechnology, Dallas, Texas (TX), USA	1:100
KRT13	Mouse, monoclonal	52 kDa	sc-101460, Santa Cruz Biotechnology, Dallas, Texas (TX), USA	1:200
PAX6	Rabbit, polyclonal	46–48 kDa	AB-2237, Merck, Darmstadt, Hessen, Germany	1:1000
RDH10	Rabbit, polyclonal	39 kDa	14644-1-AP, Proteintech, Rosemont, Illinois (IL), USA	1:1000
STRA6	Rabbit, polyclonal	73–78 kDa	22001-1-AP, Proteintech, Rosemont, Illinois (IL), USA	1:2500

4.6. ELISA (Enzyme Linked Immunosorbent Assay) of Cell Culture Supernatant

Quantification of secreted proteins in cell culture supernatants was performed using DuoSet™ ELISA kits (R&D Systems, Minneapolis, Minnesota (MN), USA), as listed in Table 4. All measurements were conducted in duplicate. Experimental samples were appropriately diluted to ensure that absorbance values fell within the linear range of detection. All procedures were performed in accordance with the manufacturer's kit- and lot-specific instructions. Briefly, 96-well microplates (R&D Systems, Minneapolis, Minnesota (MN), USA) were coated with 100 µL per well of capture antibody and incubated overnight at room temperature. Plates were then washed three times with 400 µL of wash buffer (0.05% Tween-20 in PBS) per well and blocked with 300 µL of reagent diluent (1% BSA in PBS) to prevent nonspecific binding. Subsequently, 100 µL of each supernatant sample was added and incubated under standard conditions. After washing, 100 µL of detection antibody was added to each well, followed by incubation with 100 µL of streptavidin–HRP conjugate provided with the kit. After a final washing step, 100 µL of TMB substrate solution (3,3′,5,5′-tetramethylbenzidine; 1-Step Ultra TMB-ELISA Substrate Solution, Thermo Fisher Scientific, Carlsbad, California (CA), USA) was added to each well. The reaction was terminated by adding 50 µL of 2 N H_2SO_4 per well. Optical density was measured at 450 nm with a reference wavelength of 540 nm using a Tecan Infinite 50 plate reader (Tecan Group AG, Männedorf, Switzerland) and Magellan software, version 7.5. Protein concentrations were calculated from OD values using non-linear standard curve fitting.

Table 4. List of ELISA kits used. All kits were from R&D BioTechne (Minneapolis, Minnesota (MN), USA).

Detected Protein	Catalog No./Lot No.	Range of Detection
CCL2	DY279-05/P456545	1000 pg/mL–7.8 pg/mL
CXCL1	DY275-05/P436085	2000 pg/mL–15.65 pg/mL
CXCL10	DY266-05/P432346	2000 pg/mL–15.65 pg/mL
IL-1α	DY200-05/P410705	500 pg/mL–3.90 pg/mL
IL-6	DY206-05/P437281	600 pg/mL–4.7 pg/mL
IL-8	DY208-05/P445124	2000 pg/mL–15.65 pg/mL
TNF-α	DY210-05/P452568	1000 pg/mL–7.8 pg/mL
TGF-β	DY240-05/P424503	2000 pg/mL–15.65 pg/mL
VEGFA	DY293B-05/P394527	2000 pg/mL–15.65 pg/mL

4.7. Statistical Analysis

All statistical analyses were performed using GraphPad Prism software, version 10.2.2 (GraphPad Software, San Diego, California (CA), USA). Data are presented as mean ± standard deviation (SD). Data normality was assessed using the Shapiro–Wilk test, with a significance threshold of $p = 0.05$. For data not following a normal (Gaussian) distribution, non-parametric tests, including the Mann–Whitney U test or Wilcoxon test, were applied. Comparisons between different treatment conditions were conducted using two-way ANOVA followed by Tukey's post hoc test or a two-tailed paired *t*-test as appropriate. A p-value < 0.05 was considered statistically significant. Each dataset representing an experimental condition was screened for potential outliers using Grubbs' test ($\alpha = 0.05$) with the GraphPad Prism outlier calculator. Densitometric analysis of Western blot data was performed using iBright™ Analysis Software, version 5.4.0 (Invitrogen, Carlsbad, California (CA), USA).

5. Conclusions

Our findings indicate that FOXC1 protein turnover occurs at a slower rate than transcriptional suppression, suggesting a temporal lag between mRNA downregulation and measurable protein depletion. This delay underscores a potential post-transcriptional regulation and highlights the stability of FOXC1 as a functional transcription factor. Importantly, FOXC1 appears to exert a broad regulatory control over multiple downstream pathways, integrating signals that govern inflammation, differentiation, and tissue remodeling.

Collectively, our data support a model in which FOXC1 preserves an anti-inflammatory, immune-quiescent state in pLECs, thereby preventing excessive pro-inflammatory activation under physiological conditions. Through this regulatory capacity, FOXC1 fine-tunes the interplay between TGF-β-mediated EMT, keratin expression, and inflammatory signaling, ensuring corneal epithelial integrity and homeostasis. The perturbation of FOXC1 expression disrupts this balance, predisposing the ocular surface to fibrosis, lineage instability, and inflammatory degeneration. Furthermore, our results uncover a previously unrecognized link between FOXC1 and retinoic acid metabolism in pLECs, identifying FOXC1 as a potential upstream regulator of RA-dependent epithelial maintenance. The disruption of FOXC1 alters RA flux and disturbs the proliferation–differentiation equilibrium, impairing the regenerative capacity of the limbal stem cell niche. Together, these findings position FOXC1 as a central transcriptional hub coordinating inflammatory restraint, epithelial identity, and metabolic homeostasis—processes essential for the preservation of corneal transparency and tissue renewal.

Supplementary Materials: The following supporting information can be downloaded at: https://www.mdpi.com/article/10.3390/ijms27041873/s1.

Author Contributions: Conceptualization, S.K., T.S. and N.S.; methodology, S.K., T.S. and N.S.; software, S.K., T.S. and N.S.; validation, S.K.; formal analysis, S.K.; investigation, S.K.; resources, N.S.; data curation, S.K.; writing—original draft preparation, S.K.; writing—review and editing, S.K., M.A., T.S., F.N.F., B.S., Z.L., S.L. (Shuailin Li), S.L. (Shanhe Liu), S.-L.H., S.S. and N.S.; visualization, N.S., T.S. and S.K.; supervision, N.S.; project administration, T.S. and N.S.; funding acquisition, N.S. All authors have read and agreed to the published version of the manuscript.

Funding: This research received no external funding.

Institutional Review Board Statement: The study was conducted in accordance with the Declaration of Helsinki and approved by the Ethics Committee of Saarland/Germany (No. 162/23; date of approval 9 October 2023).

Informed Consent Statement: Informed consent was obtained from all subjects involved in the study.

Data Availability Statement: Data will be made available upon reasonable request.

Acknowledgments: The work of Swarnali Kundu, Maryam Amini, Tanja Stachon, Fabian Norbert Fries, Zhen Li, Shuailin Li, Shanhe Liu, Shao-Lun Hsu, Shweta Suiwal and Nóra Szentmáry at the Dr. Rolf M. Schwiete Center for Limbal Stem Cell and Congenital Aniridia Research has been supported by the Dr. Rolf M. Schwiete Foundation. The work of Zhen Li, Shuailin Li and Shanhe Liu has been supported by the China Scholarship Council.

Conflicts of Interest: The authors declare no conflicts of interest relevant to the production and publication of this work. The funders had no role in the design of the study; in the collection, analyses, or interpretation of data; in the writing of the manuscript; or in the decision to publish the results.

Abbreviations

AAK	Aniridia associated keratopathy
ADH7	Alcohol dehydrogenase 7
ALDH3A1	Aldehyde dehydrogenase 3 family member A1
bp	Base pairs
BSA	Bovine serum albumin
CCL2	C-C motif chemokine ligand 2
CECs	Corneal epithelial cells
CXCL1	C-X-C motif chemokine ligand 1
CXCL10	C-X-C motif chemokine ligand 10
CRABP2	Cellular retinoic acid-binding protein 2
CYP1B1	Cytochrome P450 1B1
Ct	Cycle threshold (in qPCR)
Ctrl	Control/negative control
DSG1	Desmoglein 1
ECL	Enhanced chemiluminescence
ELISA	Enzyme-linked immunosorbent assay
FABP5	Fatty acid-binding protein 5
FOSL2	Fos like transcription protein 2
FOXC1	Forkhead box C1
FOXD3	Forkhead box D3
HRP	Horseradish peroxidase
IL-1α	Interleukin 1α
IL-1β	Interleukin 1β
IL-6	Interleukin 6
IL-8	Interleukin 8
KEGG	Kyoto Encyclopaedia of Genes and Genomes

KGM	Keratinocyte growth medium
KRT3	Keratin, type II cytoskeletal 3
KRT12	Keratin, type II cytoskeletal 12
KRT13	Keratin, type I cytoskeletal 13
KRT19	Keratin, type I cytoskeletal 19
LECs	Limbal epithelial cells
LSCs	Limbal stem cells
LSCD	Limbal stem cell deficiency
LPS	Lipopolysaccharide
µL	Microliter
mL	Milliliter
MAPK1	Mitogen-activated protein kinase1
MAPK3	Mitogen-activated protein kinase3
MKi67	Marker of proliferation Ki-67
MMP2	Matrix metalloproteinase-2 protein (type IV collagenase)
NFkβ	Nuclear factor kappa-light-chain-enhancer of activated B cells
OD	Optical density
PAX6	Paired box protein Pax-6
p38 MAPK	p38 Mitogen-activated protein kinase
PITX2	Paired like homeodomain transcription factor 2
pmol	Picomole
PPARγ	Peroxisome proliferator-activated receptor gamma
pg	Picogram
qRT-PCR	Quantitative Reverse Transcription Polymerase Chain Reaction
RBP1	Retinol binding protein 1
RDH10	Retinol dehydrogenase 10
SD	Standard deviation
SDS-PAGE	Sodium Dodecyl Sulfate–Polyacrylamide Gel Electrophoresis
SPINK7	Serine peptidase inhibitor, kazal type
STRA6	Signaling receptor and transporter of retinol 6
STRING	Search Tool for Retrieval of Interacting Genes/Proteins
siRNA	Small interfering RNA
TBP	TATA box binding protein
TMB	3,3′,5,5′-tetramethylbenzidine
TNF-α	Tumor necrosis factor-alpha
TGF-β	Transforming growth factor beta
TPN	Total protein normalization
TRIM44	Tripartite motif containing 44
V	Volts
VEGFA	Vascular endothelial growth factor A
YAP	Yes-associated protein

References

1. Schlötzer-Schrehardt, U.; Latta, L.; Gießl, A.; Zenkel, M.; Fries, F.N.; Käsmann-Kellner, B.; Kruse, F.E.; Seitz, B. Dysfunction of the limbal epithelial stem cell niche in aniridia-associated keratopathy. *Ocul. Surf.* **2021**, *21*, 160–173. [CrossRef]
2. Smits, J.G.A.; Cunha, D.L.; Amini, M.; Bertolin, M.; Laberthonnière, C.; Qu, J.; Owen, N.; Latta, L.; Seitz, B.; Roux, L.N.; et al. Identification of the regulatory circuit governing corneal epithelial fate determination and disease. *PLoS Biol.* **2023**, *21*, e3002336. [CrossRef] [PubMed]
3. Ouyang, H.; Xue, Y.; Lin, Y.; Zhang, X.; Xi, L.; Patel, S.; Cai, H.; Luo, J.; Zhang, M.; Zhang, M.; et al. WNT7A and PAX6 define corneal epithelium homeostasis and pathogenesis. *Nature* **2014**, *511*, 358–361. [CrossRef] [PubMed]
4. Zhu, L.; Chen, C.; Wu, S.; Guo, H.; Li, L.; Wang, L.; Liu, D.; Zhan, Y.; Du, X.; Liu, J.; et al. PAX6-WNK2 Axis Governs Corneal Epithelial Homeostasis. *Investig. Ophthalmol. Vis. Sci.* **2024**, *65*, 40. [CrossRef] [PubMed]
5. Ouyang, J.; Shen, Y.C.; Yeh, L.K.; Li, W.; Coyle, B.M.; Liu, C.-Y.; Fini, M.E. Pax6 overexpression suppresses cell proliferation and retards the cell cycle in corneal epithelial cells. *Investig. Ophthalmol. Vis. Sci.* **2006**, *47*, 2397–2407. [CrossRef]

6. Mao, Y.; Ou, S.; Zhu, C.; Lin, S.; Liu, X.; Liang, M.; Yu, J.; Wu, Y.; He, H.; Zong, R.; et al. Downregulation of p38 MAPK Signaling Pathway Ameliorates Tissue-Engineered Corneal Epithelium. *Tissue Eng. Part A* **2022**, *28*, 977–989. [CrossRef]
7. Li, Y.; Ge, L.; Ren, B.; Zhang, X.; Yin, Z.; Liu, H.; Yang, Y.; Liu, Y.; Xu, H. De-Differentiation of Corneal Epithelial Cells Into Functional Limbal Epithelial Stem Cells After the Ablation of Innate Stem Cells. *Investig. Ophthalmol. Vis. Sci.* **2024**, *65*, 32. [CrossRef]
8. Li, M.; Zhu, L.; Liu, J.; Huang, H.; Guo, H.; Wang, L.; Li, L.; Gu, S.; Tan, J.; Zhong, J.; et al. Loss of FOXC1 contributes to the corneal epithelial fate switch and pathogenesis. *Signal Transduct. Target. Ther.* **2021**, *6*, 5. [CrossRef]
9. Latta, L.; Figueiredo, F.C.; Ashery-Padan, R.; Collinson, J.; Daniels, J.; Ferrari, S.; Szentmáry, N.; Solá, S.; Shalom-Feuerstein, R.; Lako, M.; et al. Pathophysiology of aniridia-associated keratopathy: Developmental aspects and unanswered questions. *Ocul. Surf.* **2021**, *22*, 245–266. [CrossRef]
10. Lewis, C.J.; Hedberg-Buenz, A.; DeLuca, A.P.; Stone, E.M.; Alward, W.L.; Fingert, J.H. Primary congenital and developmental glaucomas. *Hum. Mol. Genet.* **2017**, *26*, R28–R36. [CrossRef]
11. Seo, S.; Singh, H.P.; Lacal, P.M.; Sasman, A.; Fatima, A.; Liu, T.; Schultz, K.M.; Losordo, D.W.; Lehmann, O.J.; Kume, T. Forkhead box transcription factor FoxC1 preserves corneal transparency by regulating vascular growth. *Proc. Natl. Acad. Sci. USA* **2012**, *109*, 2015–2020. [CrossRef]
12. Wang, X.; Shan, X.; Gregory-Evans, C.Y. A mouse model of aniridia reveals the in vivo downstream targets of Pax6 driving iris and ciliary body development in the eye. *Biochim. Biophys. Acta Mol. Basis Dis.* **2017**, *1863*, 60–67. [CrossRef] [PubMed]
13. Omatsu, Y.; Seike, M.; Sugiyama, T.; Kume, T.; Nagasawa, T. Foxc1 is a critical regulator of haematopoietic stem/progenitor cell niche formation. *Nature* **2014**, *508*, 536–540. [CrossRef] [PubMed]
14. Yang, Y.; Li, W.; Yang, H.; Zhang, Y.; Zhang, S.; Xu, F.; Hao, Y.; Cao, W.; Du, G.; Wang, J. Research progress on the regulatory mechanisms of FOXC1 expression in cancers and its role in drug resistance. *Gene* **2024**, *897*, 148079. [CrossRef] [PubMed]
15. Arcot Sadagopan, K.; Liu, G.T.; Capasso, J.E.; Wuthisiri, W.; Keep, R.B.; Levin, A.V. Anirdia-like phenotype caused by 6p25 dosage aberrations. *Am. J. Med. Genet. A* **2015**, *167*, 524–528. [CrossRef]
16. Micheal, S.; Siddiqui, S.N.; Zafar, S.N.; Villanueva-Mendoza, C.; Cortés-González, V.; Khan, M.I.; Hollander, A.I.D. A novel homozygous mutation in FOXC1 causes axenfeld Rieger syndrome with congenital glaucoma. *PLoS ONE* **2016**, *11*, e0160016. [CrossRef]
17. Ito, Y.A.; Footz, T.K.; Berry, F.B.; Mirzayans, F.; Yu, M.; Khan, A.O.; Walter, M.A. Severe molecular defects of a novel FOXC1 W152G mutation result in aniridia. *Investig. Ophthalmol. Vis. Sci.* **2009**, *50*, 3573–3579. [CrossRef]
18. François, M.; Ramchandran, R. Studies on Axenfeld-Rieger syndrome patients and mice reveal Foxc1's role in corneal neovascularization. *Proc. Natl. Acad. Sci. USA* **2012**, *109*, 1818–1819. [CrossRef]
19. Han, B.; Bhowmick, N.; Qu, Y.; Chung, S.; Giuliano, A.E.; Cui, X. FOXC1: An emerging marker and therapeutic target for cancer. *Oncogene* **2017**, *36*, 3957–3963. [CrossRef]
20. Yin, L.; Li, Q.; Mrdenovic, S.; Chu, G.C.-Y.; Wu, B.J.; Bu, H.; Duan, P.; Kim, J.; You, S.; Lewis, M.S.; et al. KRT13 promotes stemness and drives metastasis in breast cancer through a plakoglobin/c-Myc signaling pathway. *Breast Cancer Res.* **2022**, *24*, 7. [CrossRef]
21. Tibrewal, S.; Ratna, R.; Gour, A.; Agarkar, S.; Dubey, S.; Ganesh, S.; Kekunnaya, R.; Sangwan, V.; Liu, Y.; Vanita, V. Clinical and molecular aspects of congenital aniridia—A review of current concepts. *Indian J. Ophthalmol.* **2022**, *70*, 2280–2292. [CrossRef]
22. Samant, M.; Chauhan, B.K.; Lathrop, K.L.; Nischal, K.K. Congenital aniridia: Etiology, manifestations and management. *Expert Rev. Ophthalmol.* **2016**, *11*, 135–144. [CrossRef] [PubMed]
23. Landsend, E.C.S.; Utheim, Ø.A.; Pedersen, H.R.; Aass, H.C.D.; Lagali, N.; Dartt, D.A.; Baraas, R.C.; Utheim, T.P. The level of inflammatory tear cytokines is elevated in congenital Aniridia and associated with meibomian gland dysfunction. *Investig. Ophthalmol. Vis. Sci.* **2018**, *59*, 2197–2204. [CrossRef] [PubMed]
24. Ihnatko, R.; Edén, U.; Lagali, N.; Dellby, A.; Fagerholm, P. Analysis of protein composition and protein expression in the tear fluid of patients with congenital aniridia. *J. Proteom.* **2013**, *94*, 78–88. [CrossRef] [PubMed]
25. Schwanhüusser, B.; Busse, D.; Li, N.; Dittmar, G.; Schuchhardt, J.; Wolf, J.; Chen, W.; Selbach, M. Global quantification of mammalian gene expression control. *Nature* **2011**, *473*, 337–342, Erratum in *Nature* **2013**, *495*, 126–127. [CrossRef]
26. Perl, K.; Ushakov, K.; Pozniak, Y.; Yizhar-Barnea, O.; Bhonker, Y.; Shivatzki, S.; Geiger, T.; Avraham, K.B.; Shamir, R. Reduced changes in protein compared to mRNA levels across non-proliferating tissues. *BMC Genom.* **2017**, *18*, 305. [CrossRef]
27. Vogel, C.; Marcotte, E.M. Insights into the regulation of protein abundance from proteomic and transcriptomic analyses. *Nat. Rev. Genet.* **2012**, *13*, 227–232. [CrossRef]
28. Braunsperger, M.V.; Martin, G.; Herzig, T.; Kußberger, I.; Gießl, A.; Steimle, S.; Schlötzer-Schrehardt, U.; Schlunck, G.; Reinhard, T.; Polisetti, N. Proteomic Insights into Human Limbal Epithelial Progenitor-Derived Small Extracellular Vesicles. *Stem Cell Rev. Rep.* **2025**, *21*, 1578–1593. [CrossRef]

29. Ou, S.; Cai, M.; Feng, Y.; Lin, S.; Zheng, X.; Zhao, S.; Gu, H.; Wu, Y. Ocular surface health and disease: Insight from single-cell RNA sequencing. *Front. Genet.* **2025**, *16*, 1683167. [CrossRef]
30. Koo, H.-Y.; Kume, T. FoxC1-dependent regulation of vascular endothelial growth factor signaling in corneal avascularity. *Trends Cardiovasc. Med.* **2013**, *23*, 1–4. [CrossRef]
31. Bhakuni, T.; Norden, P.R.; Ujiie, N.; Tan, C.; Lee, S.K.; Tedeschi, T.; Hsieh, Y.-W.; Wang, Y.; Liu, T.; Fawzi, A.A.; et al. FOXC1 regulates endothelial CD98 (LAT1/4F2hc) expression in retinal angiogenesis and blood-retina barrier formation. *Nat. Commun.* **2024**, *15*, 4097. [CrossRef] [PubMed]
32. Ray, T.; Ryusaki, T.; Ray, P.S. Therapeutically Targeting Cancers That Overexpress FOXC1: A Transcriptional Driver of Cell Plasticity, Partial EMT and Cancer Metastasis. *Front. Oncol.* **2021**, *11*, 721959. [CrossRef] [PubMed]
33. Liu, Y.; Chen, S.; Tian, M.; Giuliano, A.; Cui, X. FOXC1 restrains NF-κB-mediated interleukin-1β transcription in breast cancer. *MedComm* **2023**, *4*, e440. [CrossRef] [PubMed]
34. Suwara, M.I.; Green, N.J.; Borthwick, L.A.; Mann, J.; Mayer-Barber, K.D.; Barron, L.; Corris, P.A.; Farrow, S.N.; Wynn, T.A.; Fisher, A.J.; et al. IL-1a released from damaged epithelial cells is sufficient and essential to trigger inflammatory responses in human lung fibroblasts. *Mucosal Immunol.* **2014**, *7*, 684–693. [CrossRef]
35. Zhou, Y.; Kato, H.; Asanoma, K.; Kondo, H.; Arima, T.; Kato, K.; Matsuda, T.; Wake, N. Identification of FOXC1 as a TGF-beta1 responsive gene and its involvement in negative regulation of cell growth. *Genomics* **2002**, *80*, 465–472. [CrossRef]
36. Zhang, H.; Nie, J.; Bao, Z.; Shi, Y.; Gong, J.; Li, H. FOXC1 promotes EMT and colorectal cancer progression by attracting M2 macrophages via the TGF-β/Smad2/3/snail pathway. *Cell. Signal.* **2025**, *130*, 111680. [CrossRef]
37. Yuan, Y.; Yeh, L.K.; Liu, H.; Liu, H.; Yamanaka, O.; Hardie, W.D.; Kao, W.W.-Y.; Liu, C.-Y. Targeted overexpression of TGF-α in the corneal epithelium of adult transgenic mice induces changes in anterior segment morphology and activates noncanonical Wnt Signaling. *Investig. Ophthalmol. Vis. Sci.* **2013**, *54*, 1829–1837. [CrossRef]
38. Yang, Z.; Jiang, S.; Cheng, Y.; Li, T.; Hu, W.; Ma, Z.; Chen, F.; Yang, Y. FOXC1 in cancer development and therapy: Deciphering its emerging and divergent roles. *Ther. Adv. Med. Oncol.* **2017**, *9*, 797–816. [CrossRef]
39. Latta, L.; Nordström, K.; Stachon, T.; Langenbucher, A.; Fries, F.N.; Szentmáry, N.; Seitz, B.; Käsmann-Kellner, B. Expression of retinoic acid signaling components ADH7 and ALDH1A1 is reduced in aniridia limbal epithelial cells and a siRNA primary cell based aniridia model. *Exp. Eye Res.* **2019**, *179*, 8–17. [CrossRef]
40. Latta, L.; Knebel, I.; Bleil, C.; Stachon, T.; Katiyar, P.; Zussy, C.; Fries, F.N.; Käsmann-Kellner, B.; Seitz, B.; Szentmáry, N. Similarities in DSG1 and KRT3 down regulation through retinoic acid treatment and PAX6 knockdown related expression profiles: Does PAX6 affect RA signaling in limbal epithelial cells? *Biomolecules* **2021**, *11*, 1651. [CrossRef]
41. Latta, L.; Viestenz, A.; Stachon, T.; Colanesi, S.; Szentmáry, N.; Seitz, B.; Käsmann-Kellner, B. Human aniridia limbal epithelial cells lack expression of keratins K3 and K12. *Exp. Eye Res.* **2018**, *167*, 100–109. [CrossRef]
42. Tian, X.; Zhang, M.; Wu, Y.; Zhang, L.; Zhang, L.; Zheng, X.; Ou, S.; Gu, H. Establishing a Severe Corneal Inflammation Model in Rats Based on Corneal Epithelium Curettage Combined with Corneal Sutures. *J. Vis. Exp.* **2024**, *213*, e67305. [CrossRef] [PubMed]
43. Nowell, C.S.; Radtke, F. Corneal epithelial stem cells and their niche at a glance. *J. Cell Sci.* **2017**, *130*, 1021–1025. [CrossRef] [PubMed]
44. Siegenthaler, J.A.; Ashique, A.M.; Zarbalis, K.; Patterson, K.P.; Hecht, J.H.; Kane, M.A.; Folias, A.E.; Choe, Y.; May, S.R.; Kume, T.; et al. Retinoic Acid from the Meninges Regulates Cortical Neuron Generation. *Cell* **2009**, *139*, 597–609. Erratum in *Cell* **2011**, *146*, 486. [CrossRef] [PubMed]
45. Como, C.N.; O'Rourke, R.; Winkler, C.; Mitchell, D.; Tran, L.; Lorberbaum, D.; Sussel, L.; Franco, S.; Siegenthaler, J. Meningeal-derived retinoic acid regulates neurogenesis via suppression of Notch and Sox2. *Cell Rep.* **2025**, *44*, 115637. [CrossRef]
46. Celik, S.D.; Ates, O. Analysis of CRABP2 and FABP5 genes in primary and recurrent pterygium tissues. *Mol. Biol. Rep.* **2020**, *47*, 6105–6110. [CrossRef]
47. Ramachandran, R.; Ibragimova, S.; Woods, L.M.; AlHouqani, T.; Gomez, R.L.; Simeoni, F.; Hachim, M.Y.; Somervaille, T.C.; Philpott, A.; Carroll, J.S.; et al. Conserved role of FOXC1 in TNBC is parallel to FOXA1 in ER+ breast cancer. *iScience* **2024**, *27*, 110500. [CrossRef]
48. Tang, X.; Liang, Y.; Sun, G.; He, Q.; Hou, Z.; Jiang, X.; Gao, P.; Qu, H. Upregulation of CRABP2 by TET1-mediated DNA hydroxymethylation attenuates mitochondrial apoptosis and promotes oxaliplatin resistance in gastric cancer. *Cell Death Dis.* **2022**, *13*, 848. [CrossRef]
49. Katiyar, P.; Stachon, T.; Fries, F.N.; Parow, F.; Ulrich, M.; Langenbucher, A.; Cayless, A.; Seitz, B.; Käsmann-Kellner, B.; Latta, L.; et al. Decreased FABP5 and DSG1 protein expression following PAX6 knockdown of differentiated human limbal epithelial cells. *Exp. Eye Res.* **2022**, *215*, 108904. [CrossRef]

50. Kundu, S.; Amini, M.; Stachon, T.; Fries, F.; Seitz, B.; Li, Z.; Li, S.; Liu, S.; Shu, S.-L.; Suiwal, S.; et al. Effect of isolated keratin 3 knockdown on gene expression of primary limbal epithelial cells without and with inflammatory stimuli. *Ann. Anat.* **2025**, *260*, 152670. [CrossRef]
51. Livak, K.J.; Schmittgen, T.D. Analysis of relative gene expression data using real-time quantitative PCR and the $2^{-\Delta\Delta CT}$ Method. *Methods* **2001**, *25*, 402–408. [CrossRef]